

Design and Application of Metal Organic Frameworks

A Major Qualifying Project Report

Submitted to the Faculty

of the

WORCESTER POLYTECHNIC INSTITUTE

in partial fulfillment of the requirements for the

Degree of Bachelor of Science

By:

Sahag Voskian _____

Date: April 28, 2011

Approved:

Professor John C. MacDonald, Primary Advisor

Professor William M. Clark, Co-Advisor

Abstract

Metal-organic frameworks (MOFs) consisting of crystalline coordination polymers are of interest as host materials for molecular storage and separation because MOFs exhibit permanent porosity, high thermal stability, and feature pores with high surface areas, large pore volumes, and properties that can be modified through synthesis. We currently are exploring the design and porous properties of a new family of porous MOFs derived from 4-(imidazol-1-yl)benzoic acids coordinated to Cu(II) or Cd(II) ions in an effort to develop highly absorbent materials for application in environmental remediation of polyaromatic hydrocarbons (PAHs). Toward that goal, the work in this project focused in two areas: (1) synthesis and characterization of several new 4-(imidazol-1-yl)benzoic acids to expand our repertoire of molecular building blocks for preparing MOFs, and (2) investigation of the ability of MOFs to absorb poly-aromatic hydrocarbons from solution. A number of new 4-(imidazol-1-yl)benzoic acid ligands were prepared featuring elongated backbones or alkyl groups substituted on the imidazole and benzene groups to determine whether the dimensions and surface properties (e.g. hydrophobicity) of pores in the resulting MOFs could be modified to promote adsorption of PAH guests. In addition, absorption of three PAHs—naphthalene, phenanthrene, and pyrene—by one of our 4-(imidazol-1-yl)benzoic acid Cd-based MOFs and Yaghi's well-known IRMOF-5 was carried out and the dynamic uptake data fitted with kinetic models for the two MOF systems. This study demonstrated that our 4-(imidazol-1-yl)benzoic acid Cd-based MOF showed up to fivefold capacity for absorbing naphthalene, phenanthrene and pyrene compared to IRMOF-5.

Acknowledgments

Advisors:

I would like to thank my chemistry advisor Professor John C. MacDonald under whose supervision I worked for more than three years. Professor MacDonald has been a great mentor who, besides supporting my research, dedicated a great amount of time guiding me on how to internalize the scientific paradigm.

I would also like to thank my chemical engineering advisor Professor William M. Clark who has been overseeing my work in chemical engineering throughout my career at WPI. Professor Clark has always supported my academic ambition and research, and has constantly guided me to viable engineering methodologies.

Faculty:

Professor James P. Dittami
Professor Anthony G. Dixon
Professor Nikolaos K. Kazantzis
Professor Christopher R. Lambert
Professor Kristin N. Wobbe

Graduate Students:

Moqing Hu
Ahsan Munir
Pranoti Navare

Machine Shop:

Jack Ferraro
Neil Whitehouse

Funding:

U.S. Army Research Office (grant # W911NF-05-0293)

Table of Contents

Abstract	i
Acknowledgments.....	ii
Table of Contents	iii
Table of Figures	iv
Table of Tables.....	vi
1. Introduction.....	1
2. Background.....	2
3. Metal-Organic Frameworks.....	12
3.1 Synthesis of Ligands.....	12
4-(Imidazol-1-yl)benzoic Acid Ligands.....	12
A Polyfunctional Ligand.....	15
3.2 Hydrothermal Synthesis of MOFs	18
4. Sorption Studies of Polyaromatic Hydrocarbons by MOFs	20
4.1. Methodology.....	22
4.2. Results and Discussion	22
Sorption Kinetics and Equilibria.....	22
Competitive Sorption Experiments.....	30
5. Conclusions.....	33
6. References.....	34

Table of Figures

Figure 1. Examples of several zeolite frameworks generated by different arrangements of the sodalite cage. ^[3]	3
Figure 2. Examples of porous MOF architectures derived from coordination complexes with indium ions. ^[6]	4
Figure 3. Structure of the porous cubic framework generated in IRMOF-5 when BDC is reacted with Zn(II) ions. ^[7]	4
Figure 4. Comparison of the cubic structures of IRMOFs formed when linear aromatic dicarboxylic acids are reacted with Zn(II) ions. Top: Increasing the length of the aromatic dicarboxylic acid (highlighted in orange) gives IRMOFs with larger channels. Bottom: Introducing substituents (highlighted in red) onto benzenedicarboxylic acid gives IRMOFs with cubic frameworks identical to that of IRMOF-5 (far left) in which the substituents protrude into the channels. ^[8]	5
Figure 5. Example of a porous, anisorecticular (non-cubic) MOF formed upon reaction of a 1:1 mixture of an aromatic dicarboxylic acid with an aromatic dipyridines in the presence of Zn(II) ions. ^[14]	7
Figure 6. Comparison between the structures of benzenedicarboxylic acid (BDC) and 4-(imidazol-1-yl)benzoic acid ligands. Coordination to metal ions occurs at the carboxylic acid (highlighted in orange) and imidazole (highlighted in blue) groups. Substituents can be introduced on the backbone of the ligands by replacing hydrogen atoms (highlighted in red) with different organic groups.	8
Figure 7. Synthetic strategy for preparing low symmetry MOFs. Reaction of substituted 4-(imidazol-1-yl)benzoic acid ligands with Cu(II) or Cd(II) metal salts (left) leads to octahedral coordination of the metal ions by carboxylate and imidazole groups in which the bonded ligands oriented either in a square-planar (top center) or distorted tetrahedral (bottom center) arrangement. Further assembly of the square-planar and tetrahedral complexes produces MOFs with different framework architectures (two possible examples of which are shown on the right).	8
Figure 8. Views showing the crystal structures and channels present in Cd- and Cu-based MOFs synthesized previously in our lab.	10
Figure 9. Views of the channels in Cu MOF-3 showing the location of methyl groups (red circles) on the imidazole ring, hydrogen atoms (blue ovals) on the benzene ring, and the backbone of the benzene rings (orange rectangles).	11
Figure 10. Structure of the 4-(imidazol-1-yl) parent ligand present in Cu MOFs-3,4,5 showing the positions of methyl, ethyl, and propyl groups (red circle) on the imidazole ring, hydrogen atoms (blue ovals) on the benzene ring, and the backbone of the benzene rings (orange rectangles).	12
Figure 11. Synthetic scheme used for acylation and esterification.	13
Figure 12. Scheme used for N-arylation.	14
Figure 13. Scheme used for esterification and photodimerization.	15
Figure 14. (a) Example of hydrothermal synthesis in which the solid MOF product forms large, single crystals suitable for crystal structure determination. (b) Example of hydrothermal synthesis in which the solid MOF product forms a microcrystalline powder.	18
Figure 15. Heating ramping and cooling scheme for the oven used to carry out hydrothermal synthesis of MOFs in sealed microwave vials.	19
Figure 16. Cap-and-stick (top) and space-filling (bottom) views of the crystal structures and channels of IRMOF-5 and Cd MOF-2.	20

Figure 17. Chemical structures, formulas, molecular weights, and molecular dimensions for naphthalene, phenanthrene, and pyrene.	21
Figure 18. Example of the Liquid-Chromatography sequence for five vials of PAH guest solutions with increasing concentrations; the injector position is indicated by the dots at different times.....	22
Figure 19. Plot of t/q against t for the sorption data for naphthalene.....	23
Figure 20. Pseudo-second-order sorption kinetics of naphthalene by IRMOF-5.	24
Figure 21. Pseudo-second-order sorption kinetics of phenanthrene by IRMOF-5.	25
Figure 22. Pseudo-second-order sorption kinetics of pyrene by IRMOF-5.....	26
Figure 23. Langmuir isotherms for the sorption of three PAHs by IRMOF-5	27
Figure 24. Pseudo-second-order sorption kinetics of naphthalene by Cd MOF-2.....	28
Figure 25. Pseudo-second-order sorption kinetics of phenanthrene by Cd MOF-2	28
Figure 26. Pseudo-second-order sorption kinetics of pyrene by Cd MOF-2.....	29
Figure 27. Langmuir isotherms for the sorption of three PAHs by Cd MOF-2.....	30
Figure 28. The linear region of the Langmuir isotherms for the sorption naphthalene and phenanthrene by IRMOF-5.....	31
Figure 29. Comparison of the number of moles of naphthalene (red) and phenanthrene (green) sorbed by IRMOF-5.....	32

Table of Tables

Table 1. Crystallographic data for methyl urocanate photodimer.....	17
Table 2. Pseudo-second-order model constants for the sorption of naphthalene by IRMOF-5 and the R^2 values	25
Table 3. Pseudo-second-order model constants for the sorption of phenanthrene by IRMOF-5 and the R^2 values	25
Table 4. Pseudo-second-order model constants for the sorption of pyrene by IRMOF-5 and the R^2 values	26
Table 5. Langmuir model constants for the sorption of three PAHs by IRMOF-5 and the R^2 values	27
Table 6. Pseudo-second-order model constants for the sorption of naphthalene by Cd MOF-2 and the R^2 values	28
Table 7. Pseudo-second-order model constants for the sorption of phenanthrene by Cd MOF-2 and the R^2 values	29
Table 8. Pseudo-second-order model constants for the sorption of pyrene by Cd MOF-2 and the R^2 values	29
Table 9. Langmuir model constants for the sorption of three PAHs by Cd MOF-2 and the R^2 values.....	30

1. Introduction

Metal-organic frameworks (MOFs) are a newly emerging class of ordered solids consisting of crystalline coordination polymers permeated by channels that impart permanent porosity. MOFs are receiving considerable attention in the chemical and materials community as host materials for molecular storage and separation because they feature channels with high surface areas and void volumes that accommodate a wide variety of organic guests. Although MOFs often are considered as organic analogues of zeolites because they share common structural and physical behavior, MOFs are unique in that they are molecular materials with properties that can be modified via organic synthesis. The vast majority of MOF structures that have been developed to date are composed of high-symmetry metal complexes containing aromatic di- and tricarboxylic acids. The most well known example is the isorecticular MOF referred to as IRMOF-5 introduced fifteen years ago by Yaghi, which has a cubic framework architecture with large 13 Å channels and an internal surface area of 4500 m²/g.

The MacDonald group has been exploring the design and porous properties of a new family of MOFs in an effort to develop coordination polymers with lower-symmetry architectures. Initial efforts have focused on developing MOFs prepared from substituted 4-(imidazol-1-yl)benzoic acid ligands coordinated to Cu(II) and Cd(II) ions. That work has produced a number of new low-symmetry MOF structures that are highly porous and that show promise as sorbents for environmental remediation of hydrophobic contaminants such as polyaromatic hydrocarbons (known carcinogens).

This project has expanded on that work in two areas. The first phase of this project focused on synthesis and characterization of seven new derivatives of 4-(imidazol-1-yl)benzoic acid to expand the library of molecular building blocks available for preparing new MOFs. The target ligands that were synthesized were chosen in order to investigate how different alkyl and aryl substituents and longer ligand backbones would affect the framework architectures and porous properties of the corresponding MOFs. Although the primary goal of this phase of the research was synthesis of new ligands, we also carried out several preliminary experiments to prepare new MOFs that produced microcrystalline solids exhibiting porous behavior. The second phase of this project involved carrying out sorption experiments with IRMOF-5 and a Cd-based MOF developed in our lab to characterize the sorption behavior and affinity of those MOFs for three polyaromatic hydrocarbon guests—naphthalene, phenanthrene, and pyrene. The primary goal of this phase of the research was to test the hypothesis that the aromatic ligands present in the channel walls of MOFs would promote sorption of aromatic guests.

Section 2 of this report provides relevant background information relating to porous materials, MOFs, and a synopsis of MOF research carried out previously in the MacDonald group. Section 3 of this report describes the synthetic strategies and experimental work carried out to produce new target ligands for MOF synthesis. Preliminary work on synthesis of frameworks is also discussed. Section 4 describes experimental work carried out to investigate the sorption behavior of MOFs and how the kinetics of sorption was modeled.

2. Background

Porous solid materials. Solids that have pores or channels permeating their structures that are large enough to permit diffusion of guest molecules, and that persist when guests are removed are referred to as porous solids. These solids usually have a porosity (fraction of void volume to the total volume occupied by the solid material) of 0.2 - 0.95. Porous materials find their way into a number of domestic, commercial and industrial applications that range from simple water purification by porous ceramics or activated carbon to energy storage, molecular storage and separation, and heterogeneous catalysis among many others.^[1] Some porous materials have penetrating open pores that connect throughout the material forming channels through which molecular guests can diffuse.^[1] Such open porous solids are of particular interest because of their utility in continuous flow and batch processes where the flow of guest molecules through channels is desirable to achieve separation or carry out reactions. The high surface area provided by the walls of the channels is known to facilitate the uptake of molecules, thereby promoting chemical reactions and other chemical processes that rely on absorption of molecules. Haphazardly arranged pores that cannot be reproduced in a repeating pattern generally result in disordered porous solids such as gels and organic polymers. Such materials have no defined structures and therefore the exact pore size and void volume cannot be characterized easily. Although the porosity (void fraction) in disordered porous materials can be modified synthetically, the dimensions and patterns of microscopic pores generally are difficult to reproduce.^[2]

Ordered porous solids. Porous crystalline solids differ from disordered porous solids in that they feature ordered microscopic pores with well-defined pore structures, dimensions and topology that can be controlled and reproduced reliably. Zeolites and metal-organic frameworks are two well know examples of ordered porous solids that have been widely studied. When synthesized under a defined set of conditions and stoichiometry of reaction components, zeolites and metal-organic frameworks exhibit consistent, predictable microstructures.^[3] The International Union of Pure and Applied Chemistry (IUPAC) classifies porous solids by the sizes of their pores.^[4] Macroporous solids have pore sizes larger than 50nm, mesoporous solids have pore sizes in the range of 2 – 50 nm and microporous solids pore sizes in the range of 0.2 – 2 nm. Microporous solids differ from the former two types in that the size of the pores is on the order of the sizes of small organic molecules. This feature imparts unique properties to microporous solids because the pores are large enough to admit guest molecules such that the walls interact with guest molecules resulting in interesting guest-host interaction dynamics and equilibria. For example, the dimensions and surface properties such as hydrophobicity or hydrophilicity of the pore walls can be tuned to interact differentially with guests and show selectivity for adsorption of certain guests on the basis of size or functional groups that are present.

Zeolites. Inorganic zeolites are one of the more ubiquitous ordered microporous materials that consist of hydrated, crystalline tectoaluminosilicates, composed of TO_4 (T = Si, Al) tetrahedra bridged by oxygen atoms. To neutralize the charges resulting from trivalent aluminum coordinated tetrahedrally by oxygen, cations of alkali and earth alkali metals are present within the channels of zeolites. Consequently, zeolites frequently are used in applications involving ion-exchange.^[3] As shown in Figure 1, zeolites exhibit a broad range of crystalline structures with different channel topologies resulting from variation in the arrangements of the sodalite cage, which is the repeating unit in zeolites. Zeolites can be synthesized by hydrothermal reaction and subsequently crystallization of reactive alkali-based aluminosilicates. The sol-

gel method also can be utilized to prepare zeolites.^[3] Surface properties such as the hydrophobicity of the channels can be controlled by varying the ratio of silicon to aluminum, which also determines the crystalline structure and pore dimensions present in the resulting zeolite. The resulting channels of zeolites are constricted by narrow openings with a maximum diameter of 4 to 12Å that restricts the utility of zeolites as porous hosts to guests consisting of ions and small organic molecules. Thus, zeolites offers a somewhat limited number of combinations of channel topology and porous properties. Nevertheless, zeolites are still used widely as porous hosts for applications that involve sorption of smaller guests (e.g., heterogeneous catalysis, molecular separation, ion exchange, etc...^[3]).

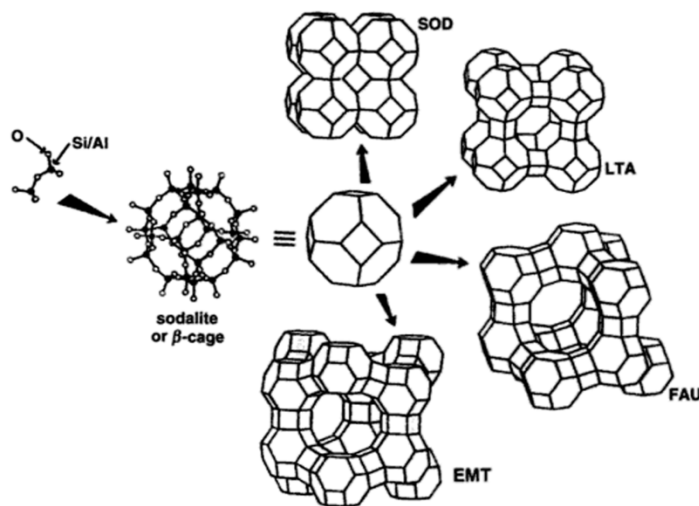


Figure 1. Examples of several zeolite frameworks generated by different arrangements of the sodalite cage.^[3]

Metal-organic frameworks (MOFs). MOFs represent a newly emerging class of ordered microporous solids whose structures and properties have been investigated over just the last 15 years. MOFs are crystalline coordination polymers that consist of metal ions or clusters to which bi-, tri- or polyfunctional rigid organic ligands coordinate, forming soluble complexes that then self-assemble into one-, two- or three dimensional frameworks. Examples of several different MOF architectures are shown in Figure 2. MOFs are “tailored nanoporous host materials” that have channels with tunable dimensions and structures and exhibit permanent porosity with large void volumes. A hallmark of MOFs is that they extremely high surface areas and void volumes that are highly accessible to organic guests.^[5] As such, MOFs represent a unique class of ordered porous materials that have a great potential as hosts in many applications that utilize porous solids.

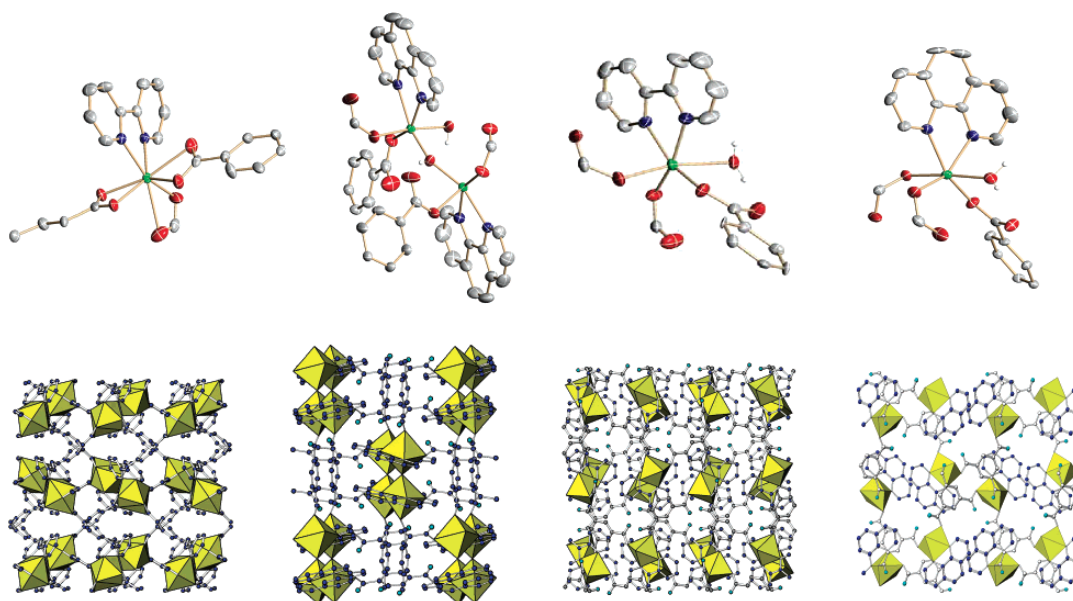


Figure 2. Examples of porous MOF architectures derived from coordination complexes with indium ions.^[6]

High symmetry MOFs based on benzenedicarboxylic acid. Isoreticular MOF-5 (IRMOF-5) is perhaps the most well-known example of a highly porous and stable MOF that serves as the standard to which the porous properties of all new MOFs are compared.^[5] IRMOF-5 was first synthesized by Yaghi in 1999 and became the corner stone for a decade of MOF research by the Yaghi group. Shown in Figure 3, the building block of IRMOF-5 consists of benzene dicarboxylic acid (BDC) ligand coordinated to tetrahedral clusters of zinc(II) ions in a BDC/Zn(II) ratio of 3:4. BDC ligands coordinate to the zinc ions at both ends via the carboxylic acid groups forming an extended cubic framework that has an internal surface area of up to 4500 m²/g.^[7]

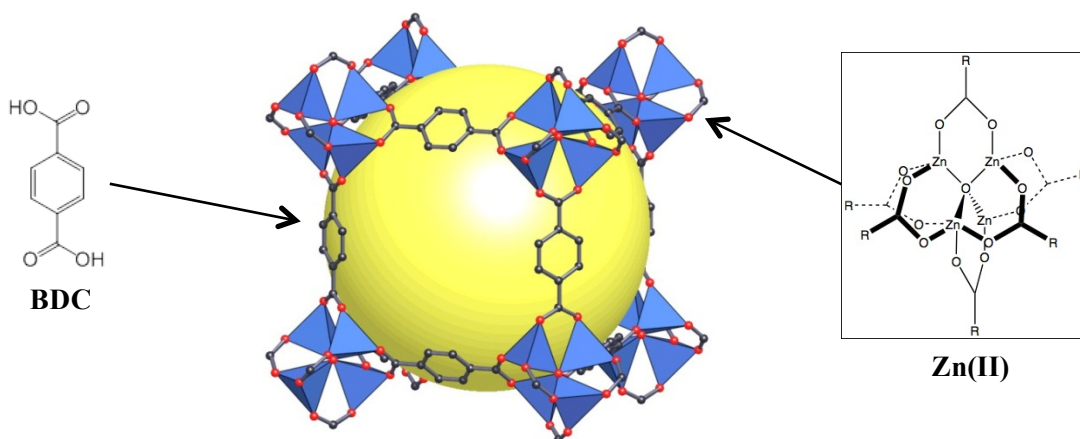


Figure 3. Structure of the porous cubic framework generated in IRMOF-5 when BDC is reacted with Zn(II) ions.^[7]

IRMOFs are tunable porous solids. One of the principle advantages of MOFs over zeolites is that the dimensions and topology of channels can be tuned through organic synthesis by modifying the molecular structure of the organic ligand that bridges the metal ions. Another advantage is that the surface properties of channels can be altered by appending different organic substituents onto the organic ligand without changing the architecture of the framework.^[8] Based on this concept, a number of variations on IRMOF-5 have been made while preserving the isorecticular cubic structure, as shown in Figure 3. For example, dicarboxylates with longer aromatic backbones (orange boxes in Figure 4) were used to generate channels with larger dimensions and void volumes. Substituted BDCs also were used to introduce polar and nonpolar functional groups that projected into the cavities. Substituting polar substituents (maroon circles in Figure 4) such as bromine or amine groups or nonpolar hydrocarbon groups such as fused benzene or cyclobutane groups in place of one or two hydrogen atoms on the benzene backbone resulted in IRMOFs with channels that were more hydrophilic or hydrophobic, respectively, than those in IRMOF5.^[8]

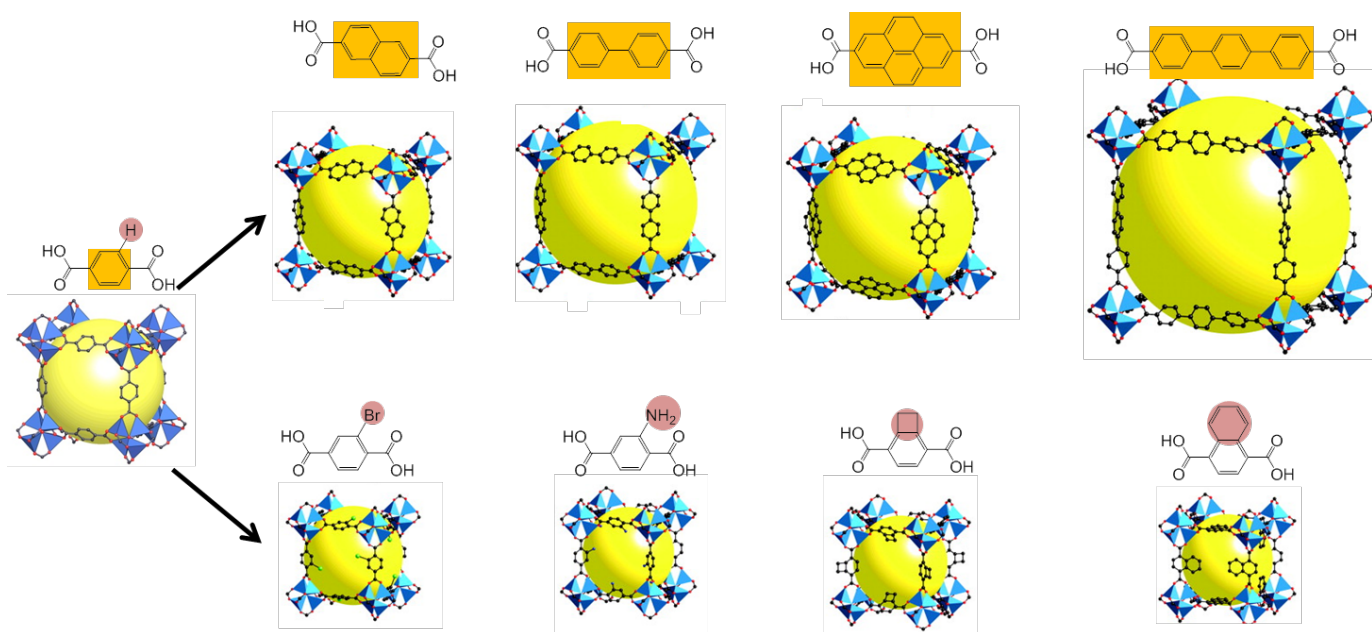


Figure 4. Comparison of the cubic structures of IRMOFs formed when linear aromatic dicarboxylic acids are reacted with Zn(II) ions. Top: Increasing the length of the aromatic dicarboxylic acid (highlighted in orange) gives IRMOFs with larger channels. Bottom: Introducing substituents (highlighted in red) onto benzenedicarboxylic acid gives IRMOFs with cubic frameworks identical to that of IRMOF-5 (far left) in which the substituents protrude into the channels.^[8]

In addition to the molecular structure of the organic ligand, the type of metal ions and coordination geometry around the metal ions plays a critical role in defining the architecture of MOFs. The vast majority of reported MOFs feature frameworks containing transition metal ions that feature ligands bound via linear, tetrahedral, square planar, or octahedral coordination geometries, while MOFs derived from lanthanide metal ions exhibit higher degrees of coordination with up to nine ligands bound to the metal ions.^[6b] The ability to tune the framework architectures and properties in MOFs via the ligand and the metal ion provides a significant advantage over the zeolites because essentially an infinite number of

variations is possible with predictable structures. However, despite the relatively high thermal stability of MOFs up to 400 °C, MOFs cannot compete with the thermal stability of zeolites, which often are stable to temperatures above 1200 °C.^[3] Nonetheless, MOFs show remarkable thermal stability for organic materials and should be of great utility as porous host materials for a wide variety of applications that do not require high temperature.

During the last decade, approximately 2200 papers describing research on MOFs have appeared in the literature. The majority of those have focused on synthesis in order to develop a robust library of MOF synthetic methodology necessary to begin exploring the properties of MOFs. The materials community only now is just beginning to fully explore the broad utility of MOFs as porous host materials. Nevertheless, interesting papers exploring the applications of MOFs are now beginning to appear with promising results.

Applications of MOFs. With the advent of a large body of synthetic protocols for preparing MOFs, researchers are now exploring the host-guest behavior of MOFs in many areas of chemistry, with the vast majority of applications focusing on the porous properties of isorecticular MOFs. For example, Yaghi and others are developing IRMOFs as host materials for energy storage. It has been shown that MOFs can be used to store high densities of hydrogen under relatively moderate pressures in steel cylinders packed with those materials.^[9] The high accessible void volume MOFs provide make them one of the more promising materials to meet hydrogen storage standards set by the DOE. Similar to zeolites, the utility of MOFs in heterogeneous catalysis has also been explored. MOFs offer the added advantage of having an organic component that can be tailored to accommodate a range of reactive groups that can actively or passively participate in catalysis.^[10] MOFs can also serve as nanoreactors that provide unique phases in which to carry out organic reactions where the large cavities of MOFs server as nanoscale containers for reactants and transition states that are too sterically demanding to fit within zeolite channels.^[11] Furthermore, MOFs with chiral framework architectures can catalyze reactions enantioselectively.^[12] Molecular sorption is an additional area where the large surface areas, pore dimensions and high porosities of MOFs provide unique opportunities. The ability of MOFs to act as sorbants is invaluable for environmental remediation and purification. Other applications that have been explored include molecular separation, molecular sensing and nanofabrication.^[13]

Lower symmetry MOFs. The majority of the known MOFs have isorecticular cubic frameworks; Yaghi's IRMOFs are the classical examples. The design of MOFs with non-cubic structures is now being investigated in an effort to expand the library of framework architectures that are available and determine whether MOFs with lower symmetries exhibit unique porous properties. Efforts to produce stable MOFs with lower symmetry focus largely on several related approaches that include utilizing nonlinear ligands instead of rigid linear dicarboxylates, asymmetrical ligands containing two differing metal-binding groups, or mixtures of two different symmetrical ligands. For example, Hupp reported a porous MOF composed of a 1:1 mixture of 1,6-naphthalene dicarboxylic acid and N',N-di-(4-pyridyl)-1,4,5,8-naphthalenetetracarboxydiimide. That MOF featured an anisorecticular, lower symmetry architecture as shown in Figure 5.^[14]

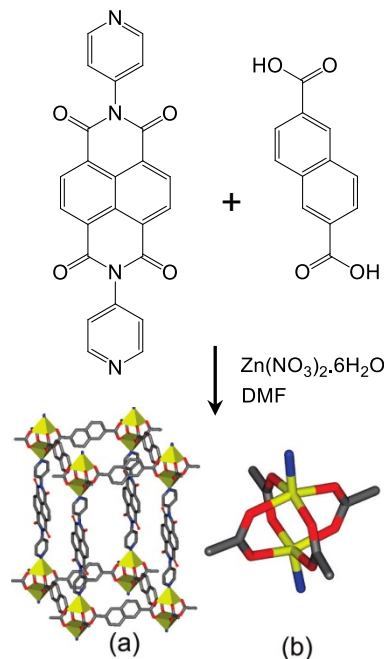


Figure 5. Example of a porous, anisorecticular (non-cubic) MOF formed upon reaction of a 1:1 mixture of an aromatic dicarboxylic acid with an aromatic dipyridines in the presence of Zn(II) ions.^[14]

Current research in the MacDonald group. Our lab has been conducting basic research in developing methods to synthesize low symmetry MOFs, analyze their framework architectures and explore the utility of MOFs in sorption of guest molecules. The MOFs being studied mainly use 4-(imidazol-1-yl)benzoic acid ligands. This ligand was chosen because it has an asymmetrical structure and two binding sites capable of coordinating to metal ions. As shown in Figure 6, the 4-(imidazol-1-yl)benzoic acid skeleton bears a carboxylate group (shown in orange) similar to BDC that is capable of bidentate binding at both oxygen atoms. The opposite end of the ligand contains an imidazole group (shown in blue) with an exposed aryl nitrogen atom that is capable of monodentate binding. Imidazoles are known to be good bases and metal coordinators. They are present in the side-chain of histidine, which is known to act as a strong metal-binding group in many metalloproteins. The presence of imidazole on the ligand introduces three additional sites (shown in maroon) at which substituents can be introduced on the backbone to modify the surface-properties of channels in MOFs. Imidazole also introduces rotational freedom around the C-N aryl bond that can result in changes in molecular conformation that lead to variation in the MOF architecture. We have demonstrated recently that mixed coordination by the carboxylate group and imidazole ring nitrogen, and the bent geometry of this ligand results in a rich variety of framework architectures of lower symmetry than the isorecticular MOFs reported by Yaghi and others. The structures of several MOFs derived from 4-(imidazol-1-yl)benzoic acid are described below.

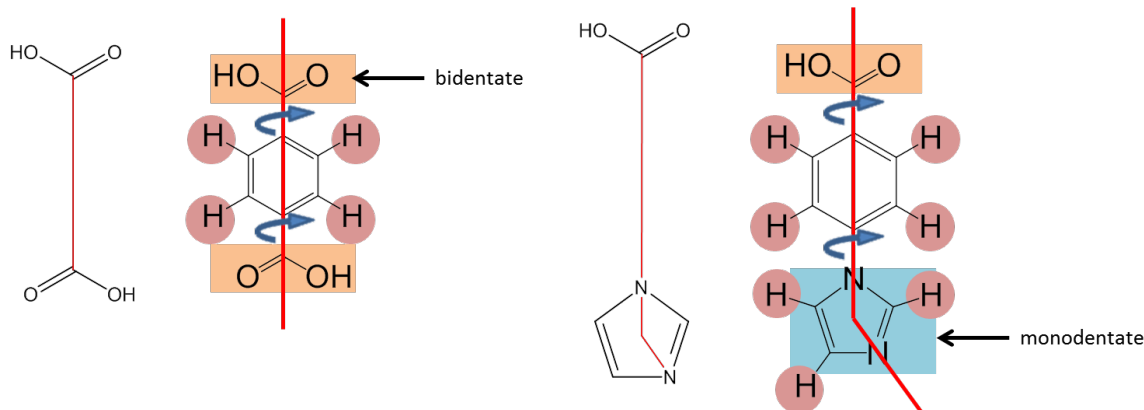


Figure 6. Comparison between the structures of benzenedicarboxylic acid (BDC) and 4-(imidazol-1-yl)benzoic acid ligands. Coordination to metal ions occurs at the carboxylic acid (highlighted in orange) and imidazole (highlighted in blue) groups. Substituents can be introduced on the backbone of the ligands by replacing hydrogen atoms (highlighted in red) with different organic groups.

A number of copper and cadmium MOFs have been successfully synthesized using the parent 4-(imidazol-1-yl)benzoic acid and substituted derivatives, as shown on the left in Figure 7. The synthesis of those MOFs was carried out in solution either at room temperature using the free carboxylic acid, or hydrothermally using a protected carboxylic acid (i.e., an ethyl ester) by slowly deprotecting the acid group via hydrolysis at elevated temperature to control the rate of reaction and subsequent growth of crystalline MOF products. As shown in the center of Figure 7, octahedral coordination of Cu(II) or Cd(II) metal ions produced two different isomeric arrangements of the bound ligands in which the ligands were oriented either in a square-planar or a distorted tetrahedral arrangement. Those coordination motifs resulted in a range of frameworks, the most common of which are illustrated schematically on the right in Figure 7.

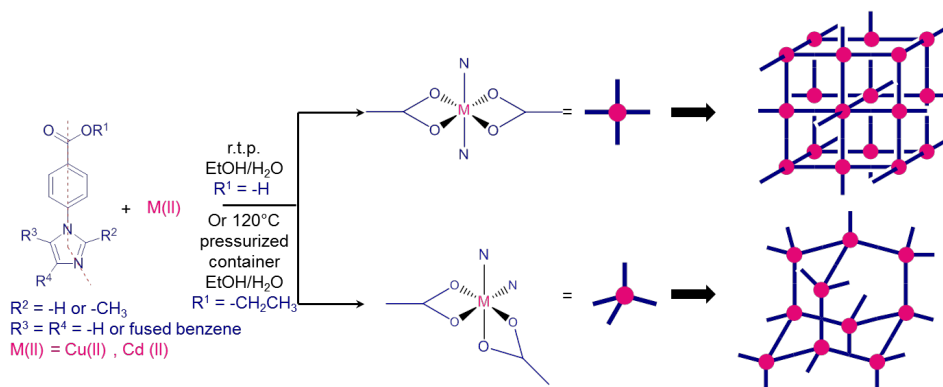


Figure 7. Synthetic strategy for preparing low symmetry MOFs. Reaction of substituted 4-(imidazol-1-yl)benzoic acid ligands with Cu(II) or Cd(II) metal salts (left) leads to octahedral coordination of the metal ions by carboxylate and imidazole groups in which the bonded ligands oriented either in a square-planar (top center) or distorted tetrahedral (bottom center) arrangement. Further assembly of the square-planar and tetrahedral complexes produces MOFs with different framework architectures (two possible examples of which are shown on the right).

Shown in Figure 8, the crystal structures of two Cd(II)-based MOFs (Cd MOF-1 and Cd-MOF-2) and three Cu(II)-based MOFs (Cu MOF-1, Cu MOF-2, and Cu MOF-3) all have non-cubic frameworks that exhibit permanent porosity resulting from large channels (up to 12 Å in diameter) that permeate the MOF structure. Porosity of all MOFs was confirmed using thermogravimetric analysis (TGA) to measure the percentage weight loss of guest solvents by thermogravimetric analysis (TGA). Guests consisting of molecules of water and ethanol that were included in the framework during synthesis accounted for 12-30% loss in mass when samples of MOFs were heated, demonstrating porosity comparable to that reported for IRMOFs. The non-cubic architectures of the MOFs shown in Figure 8 resulted in part due to the bent nature of the ligands and the resulting low-symmetry coordination geometries of the carboxylate and imidazole groups around the central metal ions.

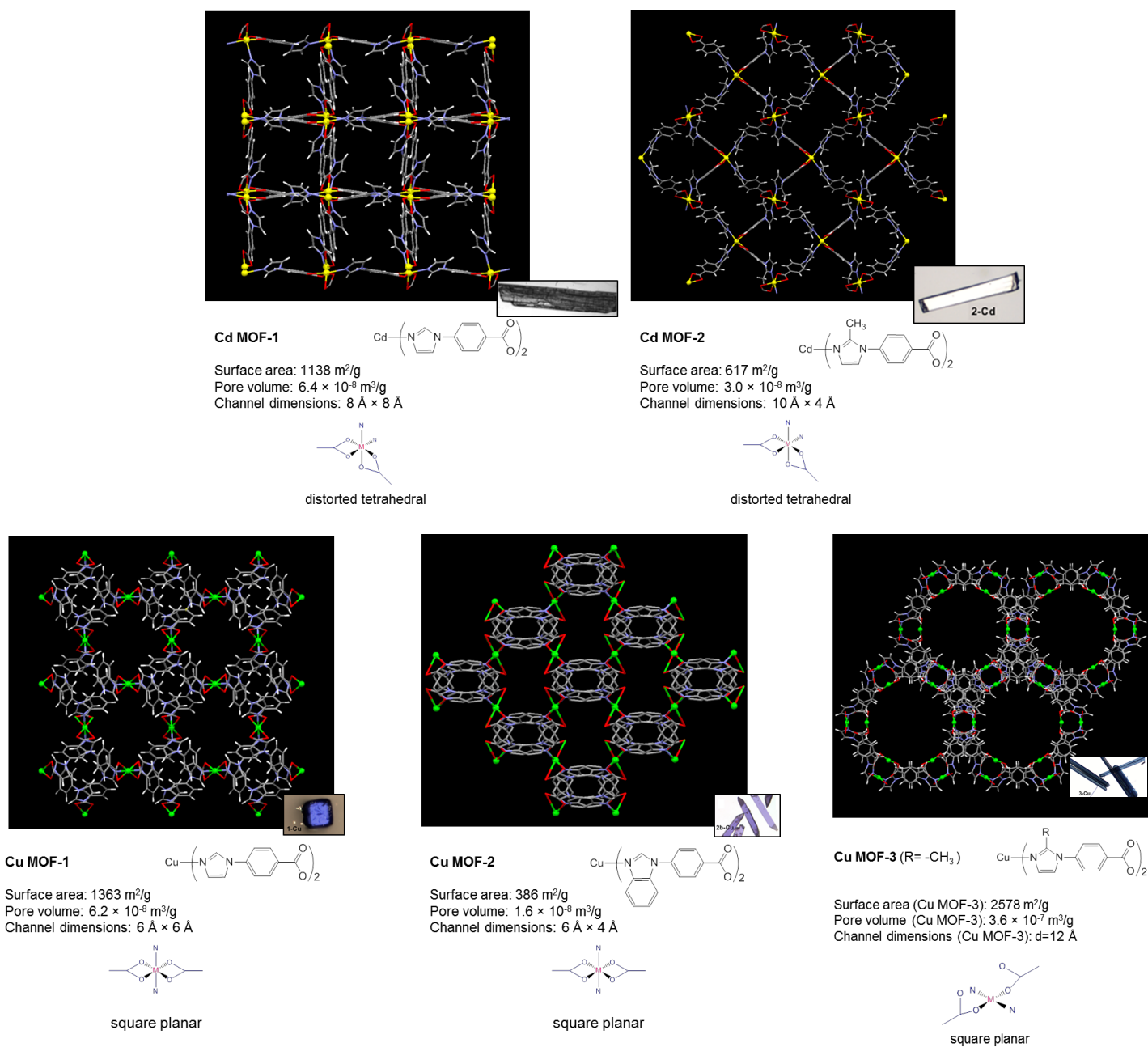


Figure 8. Views showing the crystal structures and channels present in Cd- and Cu-based MOFs synthesized previously in our lab.

Of the structures shown, Cu MOF-3 demonstrated the highest level of porosity (30% weight loss) resulting from the presence of large helical channels. Coordination of Cu ions by 4-(2-methylimidazol-1-yl)benzoic acid ligand in Cu MOF-3 was somewhat unusual in that the methyl groups close to the coordination centers created significant steric hindrance that forced the carboxylates to behave as monodentate rather than bidentate binders. Monodentate binding of the two carboxylates and two imidazole groups resulted in square-planar coordination with the four attached ligands bending to one side

of the square plane. That arrangement produced a hexagonal helical framework with 12\AA diameter channels, as shown in Figure 9. It was determined that the steric bulk of the methyl group and other longer chain alkyl groups substituted on carbon 2 of imidazole (carbon between the two nitrogen atoms on the imidazole ring) was crucial for obtaining this unique architecture. Analysis of the crystal structure of Cu MOF-3 (Figure 9) reveals that the methyl group at the 2-position of the imidazole (shown in red circles) and the hydrogen atoms at the 2,3-positions (shown in blue ovals) of the benzene ring protrude into the channels. The presence of those substituents at the surface of the channels suggested that it might be possible to introduce larger substituents on both the imidazole and benzene rings as a way to modify the surface properties of the channels without perturbing the framework structure. Similar to IRMOF-5, where the original MOF architecture is preserved across a range substituents on the benzene ring, we wanted to test whether introducing different substituents on the 4-(2-methylimidazol-1-yl)benzoic acid ligand would impart different properties to the channels. We hypothesized longer or larger alkyl substituents present on imidazole or benzene would protrude into the framework channels making them more hydrophobic. To test that hypothesis, the structures of two additional MOFs, Cu MOF-4 (R = $-\text{CH}_2\text{CH}_3$) and Cu MOF-5 (R = $-\text{CH}_2\text{CH}_2\text{CH}_3$), were synthesized in our lab using 4-(2-ethylimidazol-1-yl)benzoic acid and 4-(2-propylimidazol-1-yl)benzoic acid ligands. Analysis of the crystal structures of those MOFs (not shown) had coordination geometries, channel structures and framework architectures identical to that of Cu MOF-3 in which the alkyl substituents protruded into the framework channels. The concept of being able to control the hydrophobicity of channels is of particular interest as a potential means to increase the affinity of our MOFs toward absorbing hydrophobic guest molecules. Later in this report we describe the results of a series of sorption experiments in which we investigated the affinity and sorption characteristics of MOFs toward the hydrophobic polyaromatic hydrocarbons naphthalene, phenanthrene, and pyrene.

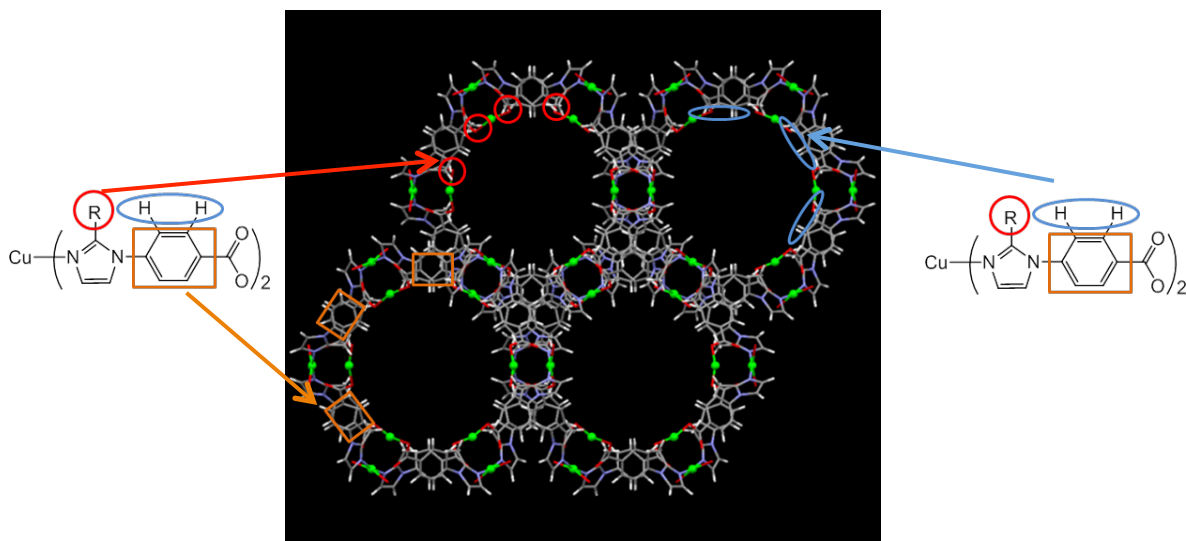


Figure 9. Views of the channels in Cu MOF-3 showing the location of methyl groups (red circles) on the imidazole ring, hydrogen atoms (blue ovals) on the benzene ring, and the backbone of the benzene rings (orange rectangles).

3. Metal-Organic Frameworks

3.1 Synthesis of Ligands

4-(Imidazol-1-yl)benzoic Acid Ligands

As described in the previous section, substitution of increasingly longer alkyl (i.e., methyl, ethyl, and propyl) groups on the imidazole ring in the parent ligand produced three copper-based MOFs with a common framework architecture (Cu MOF-3, Cu MOF-4, and Cu MOF-5). On that basis, we were interested in answering the following two questions: 1) is the Cu MOF-3 architecture maintained when substituents are introduced at other locations on the backbone of the ligand; and 2) can the diameter of channels be increased while maintaining the same framework architecture by increasing the length of the aryl components within the backbone? Accordingly, the work described in this section focused on synthesizing a number of derivatives of 4-(2-alkylimidazol-1-yl)benzoic acid (alkyl = H, CH₃, or CH₂CH₃, red in Figure 10) with simple alkyl and aryl groups substituted on the benzene ring, (blue in Figure 10) or with a longer aryl backbone (orange in Figure 10). This research was done as a first step toward expanding our library of MOFs exhibiting the hexagonal helical framework architecture and to investigate the robustness of that architecture with regard to changes in the steric demand of substituents and length of the ligand backbone. Therefore, the immediate goal was to synthesize and characterize the small library of substituted derivatives of 4-(imidazol-1-yl)benzoic acid shown in Figure 10. Ultimately, we intend to utilize those ligands to synthesize a series of Cu MOFs, solve the crystal structures to determine if a consistent Cu MOF-3 type framework is maintained, and investigate their porous behavior with respect to sorption of hydrophobic polyaromatic hydrocarbons. Although the main focus in this phase of the research was synthesis of the ligands, we attempted to prepare MOFs from several ligands and provide preliminary data indicating that porous solids were obtained. We currently are in the process of systematically testing each ligand to determine whether MOFs can be obtained.

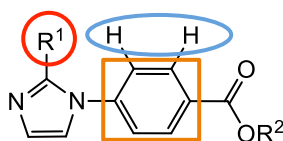


Figure 10. Structure of the 4-(imidazol-1-yl) parent ligand present in Cu MOFs-3,4,5 showing the positions of methyl, ethyl, and propyl groups (red circle) on the imidazole ring, hydrogen atoms (blue ovals) on the benzene ring, and the backbone of the benzene rings (orange rectangles).

Toward those goals, seven new substituted 4-(imidazol-1-yl)benzoic acid ligands, **1-7** (Figure 10), were synthesized. The proposed variation in molecular structure was carried out by adding the indicated alkyl or aryl substituents at the 2-position of the imidazole (in red circles) and the 2,3-positions of the benzene ring (in blue circles) and by lengthening the ligand backbone (in orange rectangle) while maintaining the orientation of the carboxylate and imidazole groups.

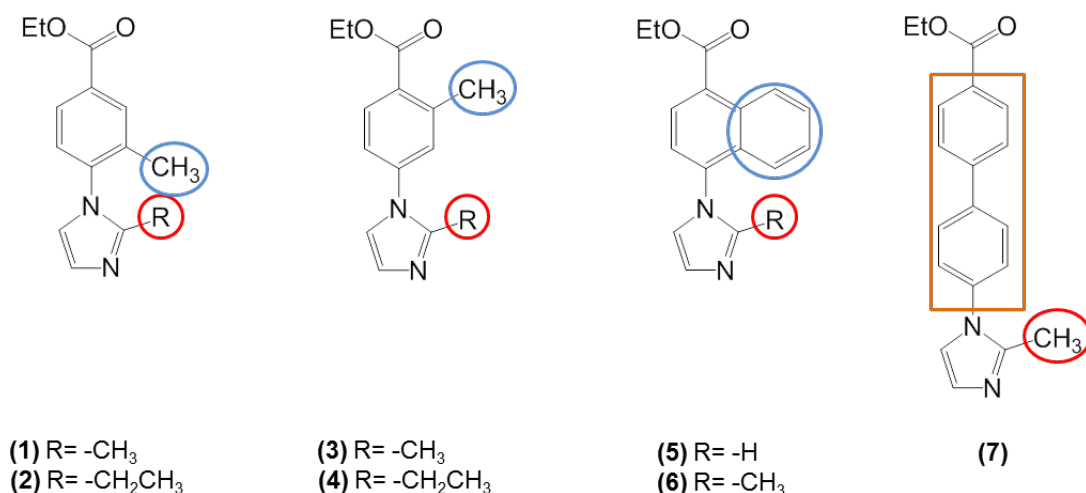


Figure 11. The structures of seven new substituted 4-(imidazol-1-yl)benzoic acid ligands that synthesized.

Ligands **1-7** were prepared in three steps using synthetic procedures modified slightly from those reported by Morgan for making the unsubstituted parent ligand as follows:^[15]

Acylation and esterification:

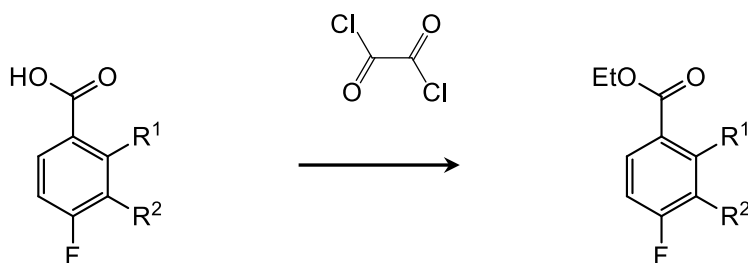


Figure 11. Synthetic scheme used for acylation and esterification.

The corresponding 4-fluoro-acid (**a**) (1.0 mmol) was dissolved in 10 ml chloroform in a round-bottom flask and the solution heated to reflux. Oxalyl chloride (5.0 mmol) was added dropwise over 5 min, the solution was allowed to reflux for 2 hrs with continuous stirring, then was cooled to RT and concentrated under vacuum. The crude solid acyl chloride product was washed with chloroform over filter paper and then transferred to a clean flask containing 20 mL of ethanol. The solution was heated at reflux for 2 hrs, then was cooled, and the resulting solution was concentrated under vacuum. The crude product was purified by column chromatography using 9:1 hexanes:ethyl acetate (v:v), $R_f \sim 0.8$.

N-Arylation:

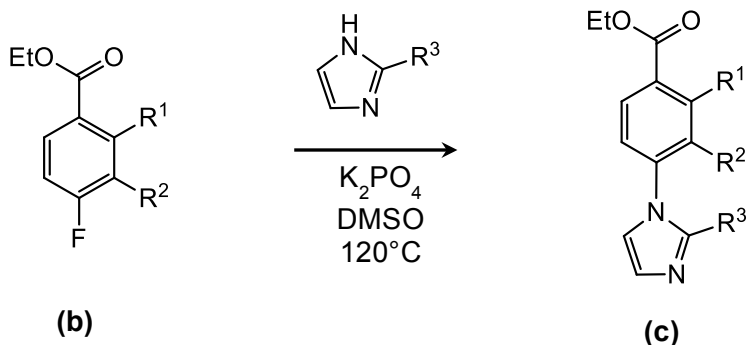


Figure 12. Scheme used for N-arylation.

The corresponding 4-fluoro-ester **(b)** (1.0 mmol) was dissolved in 10 ml DMSO in a round-bottom flask. Potassium phosphate (2.0 mmol) and imidazole (1.5 mmol) were added to the solution. The solution was heated to 120°C with continuous stirring for 2 days under a nitrogen atmosphere. The reaction mixture was then cooled to RT, quenched with 20 mL water, and extracted with ethyl acetate (4×20 mL). The organic layer was washed with brine and dried over anhydrous sodium sulfate. The suspension was filtered and the filtrate was concentrated under vacuum. The concentrate was purified by column chromatography using 19:1 ethyl acetate:methanol (v:v), $R_f \sim 0.32$.

The overall yields for ligands **1-7** were less than 20%.

The ^1H NMR spectra for ligands **1-7** were recorded in CDCl_3 using a 500MHz Bruker NMR.

Ethyl 3-methyl-4-(2-methylimidazol-1-yl)benzoate (1):

Off-white solid; ^1H NMR (500 MHz, CDCl_3): $\delta = 7.98$ (s, 1 H), 7.91 (d, 1 H), 7.20 (s, 1 H), 7.06 (s, 1 H), 6.82 (s, 1 H), 4.35 (q, 2 H), 2.14 (s, 3 H), 2.05 (s, 3 H), 1.35 (t, 3 H).

Ethyl 4-(2-ethylimidazol-1-yl)-3-methylbenzoate (2):

Off-white solid; ^1H NMR (500 MHz, CDCl_3): $\delta = 7.97$ (d, 1 H), 7.11 (s, 2 H), 6.98 (s, 1 H), 6.95 (s, 1 H), 4.33 (q, 2 H), 2.59 (s, 3 H), 2.33 (s, 3 H), 1.35 (t, 3 H).

Ethyl 2-methyl-4-(2-methylimidazol-1-yl)benzoate (3):

Pale yellow solid; ^1H NMR (500 MHz, CDCl_3): $\delta = 7.99$ (s, 1 H), 7.93 (d, 1 H), 7.18 (s, 1 H), 7.08 (s, 1 H), 6.80 (s, 1 H), 4.33 (q, 2 H), 2.12 (s, 3 H), 2.04 (s, 3 H), 1.37 (t, 3 H).

Ethyl 4-(2-ethylimidazol-1-yl)-2-methylbenzoate (4):

Pale yellow solid; ^1H NMR (500 MHz, CDCl_3): $\delta = 7.97$ (s, 1 H), 7.90 (d, 1 H), 7.20 (s, 1 H), 7.05 (s, 1 H), 6.89 (s, 1 H), 4.35 (q, 2 H), 2.39 (q, 2 H), 2.04 (s, 3 H), 1.35 (t, 3 H), 1.13 (t, 3 H).

Ethyl 4-(imidazol-1-yl)-1-naphthoate (5):

Pale pink solid; ¹H NMR (500 MHz, CDCl₃): δ= 9.00 (d, 1 H), 8.22 (d, 1 H), 7.79 (s, 1 H), 1.63 (m, 2 H), 7.59 (t, 1 H), 7.49 (d, 1 H), 7.33 (s, 1 H), 7.28 (s, 1 H), 4.52 (q, 2 H), 2.05 (s, 3 H), 1.48 (t, 3 H).

Ethyl 4-(2-methylimidazol-1-yl)-1-naphthoate (6):

Pale pink solid; ¹H NMR (500 MHz, CDCl₃): δ= 8.97 (d, 1 H), 8.23 (d, 1 H), 7.70 (t, 1H), 7.56 (t, 1 H), 7.48 (d, 1 H), 7.35 (d, 1 H), 7.18 (s, 1 H), 7.06 (s, 1 H), 4.53 (q, 2 H), 2.17 (s, 3 H), 2.05 (s, 3 H), 1.49 (t, 3 H).

Ethyl 4'-(2-methylimidazol-1-yl)-[1,1'-biphenyl]-4-carboxylate (7):

White solid; ¹H NMR (500 MHz, CDCl₃): δ= 8.09 (d, 2H), 7.64 (m, 4H), 7.33 (d, 2 H), 6.99 (s, 2 H), 4.35 (q, 2 H), 2.35 (s, 3 H), 1.36 (t, 3 H).

A Polyfunctional Ligand

In addition to investigating the utility of 4-(imidazol-1-yl)benzoic acids as ligands for preparing MOFs, we wanted to explore the possibility of synthesizing MOFs using polyfunctional ligands functionalized with two imidazole and two carboxylic acid moieties. Although we did not expect such polyfunctional ligands to form a helical framework, we were curious to determine whether reaction of such ligands would yield porous MOFs. Accordingly, we chose to investigate photodimerization of urocanic acid as a possible synthetic strategy to prepare the corresponding tetrasubstituted cyclobutane photodimer, **c**, shown in Figure 14. The photodimer was attractive as a candidate for making MOFs because it contains two carboxylate and two imidazole functionalities tethered to a rigid central ring. Although structurally from ligands **1-7**, the positions and orientation of the opposing carboxylic acid and imidazole groups along the diagonal of the cyclobutane ring are similar to those present in -(imidazol-1-yl)benzoic acids. Urocanic acid also provided an additional binding site in the form of the 2° amino nitrogen atom on imidazole ring. Moreover, MOFs utilizing urocanic acid as the linking ligand have been reported previously.^[16] Toward that end, the photodimer of urocanic acid ester was synthesized via [2+2] cycloaddition using 280 nm UV light according to the procedure below.

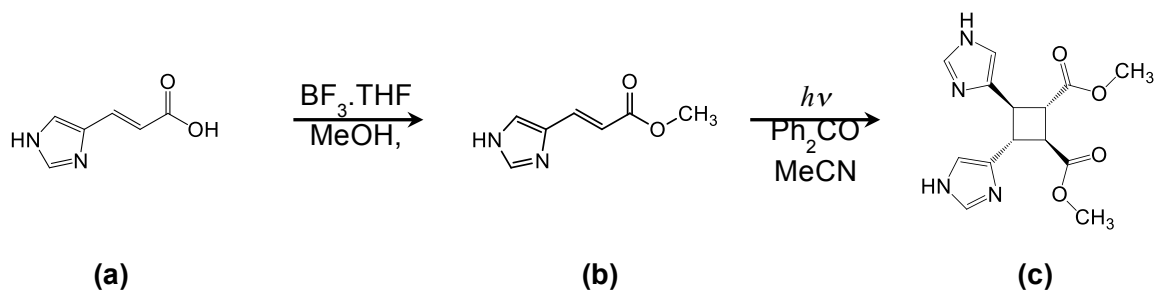
Photodimerization:

Figure 13. Scheme used for esterification and photodimerization.

Urocanic acid (**a**) (3.0 g) was dissolved in 60 mL of methanol in a round-bottom flask. Boron trifluoride diethyl ether complex solution (8.3 mL) was added and the solution was heated at reflux under a nitrogen atmosphere for 24 hrs. After cooling to RT, the solution was washed with 30 mL of 15% aqueous sodium carbonate, extracted with dichloromethane (10×10mL), and the organic layer was dried over anhydrous sodium sulfate. The suspension was then filtered and the filtrate was concentrated under vacuum. The concentrate was purified by column chromatography with ethyl acetate, $R_f \sim 0.26$. The yield of methyl urocanate (**b**) was 83%.

Methyl urocanate (**b**) (1.8 g) was dissolved in 250 mL of acetonitrile. Benzophenone (0.52 g) was added and the solution was stirred at RT under a nitrogen atmosphere for 1 hr. The solution was then irradiated with 280 nm UV light (450W low pressure mercury Hanovia UV lamp) for 60 hrs with continuous stirring under a nitrogen atmosphere, during which the solution turned dark orange and a precipitate formed. The suspension was filtered and the solid was washed with water and ethanol. The ^1H NMR spectrum of (**c**) in DMSO-d_6 was recorded δ : 12.11 (s, 2H), 7.98 (s, 2H), 7.25 (s, 2H), 4.2 (s, 6H), 3.92 (m, 2H), 3.17 (m, 2H). The photodimer (**c**) was then recrystallized from a hot solution of ethanol and water to yield pale yellow needle shaped crystals.

The crystal structure of the methyl urocanate photodimer was solved to determine the absolute stereochemistry and substitution pattern of the imidazole and carboxylic acid ester groups on the cyclobutane ring unambiguously. The following experimental procedures are used to collect the X-ray diffraction data and solve the crystal structure. A single crystal of the photodimer covered in paratone oil on 100 μ MiTeGen polyimide micromounts were mounted on a Bruker-AXS Kappa APEX CCD diffractometer equipped with an LT-II low temperature device. Diffraction data were collected at 100(2) K using graphite monochromated Mo- K_α radiation ($\lambda = 0.71073 \text{ \AA}$) using the omega scan technique. Empirical absorption corrections were applied using the SADABS program. The unit cell and space group were determined using the SAINT+ program. The structure was solved by direct methods and refined by full matrix least-squares using the SHELXTL program. Refinement was based on F^2 using all reflections. All non-hydrogen atoms were refined anisotropically. Hydrogen atoms on carbon atoms were all located in the difference maps and subsequently placed at idealized positions and given isotropic U values 1.2 times that of the carbon atom to which they were bonded. Hydrogen atoms bonded to nitrogen atoms were located and refined with isotropic thermal parameters. Mercury 1.4.2 software was used to examine the molecular structure in the solved crystal structure. The crystallographic data is shown in Table 1.

Table 1. Crystallographic data for methyl urocanate photodimer.

Formula	C ₁₄ H ₁₆ N ₄ O ₄
Formula weight	304.31
Crystal system	Tetragonal
Space group	I4 ₁ /a
Crystal color	Pale yellow
<i>a</i> (Å)	13.7828(6)
<i>b</i> (Å)	13.7828(6)
<i>c</i> (Å)	15.2100(19)
α (°)	90
β (°)	90
γ (°)	90
<i>V</i> (Å ³)	2889.38
<i>Z</i>	8
<i>D</i> _{calc} (g/cm ³)	1.399
No. reflns	7380
<i>R</i>	0.0604
<i>wR</i> ²	0.1285

Analysis of the crystal structure of the methyl urocanate photodimer revealed that the photoreaction exclusively produced the (1*R*,2*R*,3*S*,4*S*)-dimethyl 3,4-di(imidazol-4-yl)cyclobutane-1,2-dicarboxylate product shown in Figure 15. That photodimer product featured an all *trans* substitution pattern with adjacent ester and imidazole groups at the 1,2- and 3,4-positions, respectively. This photodimer has not yet been tested to determine whether it will react with Cu(II) or Cd(II) salts under hydrothermal conditions to form MOFs.

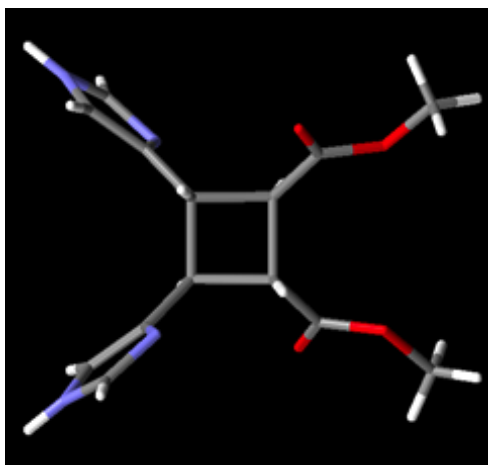


Figure 15. Crystal structure of the methyl urocanate photodimer.

3.2 Hydrothermal Synthesis of MOFs

The major thrust of this phase of the project focused on the synthesis of ligands that ultimately we hope can be used to synthesize MOFs with framework architecture identical to that of Cu MOF-3. Although we have yet to systematically test the reactivity of ligands **1-7** with Cu(II) ions under hydrothermal conditions in order to optimize conditions to produce MOFs, preliminary reactions with several ligands were carried out to test the possibility of synthesizing MOFs. The following general procedure was used.

The ligand was dissolved with the metal salt in a 2:1 molar ratio because the octahedral coordination geometry and the orientation of the ligands in MOFs synthesized previously in our group dictate that two ligand molecules will coordinate to each metal ion. The metal nitrates of Cu(II) and Cd(II) were tested. The solvent system used was 1:1 ethanol:water (v:v) based on our previous success at forming MOFs with that solvent mixture. Several reactions that were carried out at RT using the free acid ligand immediately produced insoluble precipitates when solutions containing the ligand and the metal salts were mixed. Similar experiments conducted previously in our lab revealed that reaction of 4-(imidazol-1-yl)benzoic acid ligands free carboxylic acids instead of acids protected as esters frequently formed insoluble precipitates upon contact with solutions of Cu(II) and Cd(II) metal ions. From analysis of those precipitates by powder X-ray diffraction and thermogravimetric analysis it was determined that MOFs had formed, but precipitated as microcrystalline solids due to rapid, uncontrolled coordination by the free acids. On the basis of those findings, it is likely that the precipitates observed upon reaction ligands with free acids in this study also were microcrystalline MOFs. A typical example of a microcrystalline MOF precipitate is shown in Figure 14 (b).

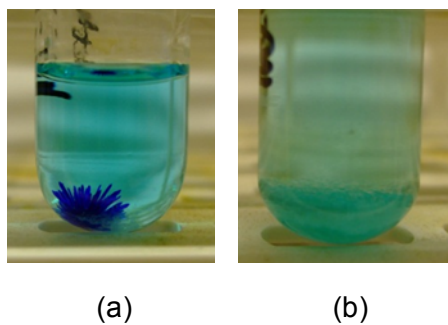


Figure 14. a) Example of hydrothermal synthesis in which the solid MOF product forms large, single crystals suitable for crystal structure determination. (b) Example of hydrothermal synthesis in which the solid MOF product forms a microcrystalline powder.

Attempts also were carried out to synthesize MOFs hydro(solvo)thermally. Those reactions were carried out by placing a 2:1 ratio of ester-protected ligands and Cu(II) or Cd(II) metal salts in 1:1 ethanol:water (v:v) in thick-walled microwave flasks sealed with aluminum caps that were then heated. Hydrothermal synthesis provided the advantage of heating the solution to temperatures higher than the boiling points of the solvents, which is known to enhance the solubility of coordination polymers as they assemble in solution and also to inhibit immediate precipitation of MOFs. Under hydrothermal conditions, the ester is

hydrolyzed slowly over hours or days to form the corresponding free carboxylic acid, which is present in low enough concentration to slow the kinetics of MOF formation. Slower assembly of coordination polymers enhances the odds of obtaining large single crystals of MOFs that are suitable for resolving the crystal structure. A typical example of large single MOF crystals formed under hydrothermal conditions is shown in Figure 14 (a). The hydrothermal synthesis experiments were carried out in a Yamato DKN 400 programmable mechanical convection oven. Use of a programmable oven allowed precise control over the heating and cooling rates for sample, which were adjusted to favor single crystal formation. Figure 15 shows the heating scheme used for hydrothermal synthesis experiments.

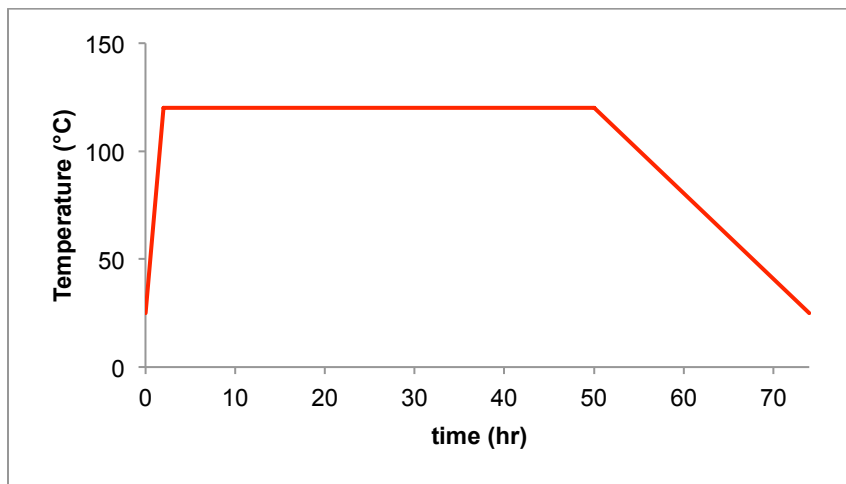


Figure 15. Heating ramping and cooling scheme for the oven used to carry out hydrothermal synthesis of MOFs in sealed microwave vials.

All of the trial hydrothermal synthesis experiments carried out with ligands **1-7** resulted in microcrystalline powders that were analyzed by TGA in platinum pans using a TA instrument, Hi-Res TGA 2950 Thermo Gravimetric Analyzer at a heating rate of 10 °C/min over a temperature range from RT to 300°C under a nitrogen atmosphere. All powder samples were recovered from solutions by pipette and were pressed dry on Whatman filter paper. Losses of up to 15 weight % were observed for several microcrystalline samples, indicating that solvent guest molecules included during synthesis were lost upon heating. Considering that water trapped in nonporous organic crystals such as monohydrates typically accounts for 2-3 weight % loss of mass, the observed losses of up to 15 weight % provide strong evidence that the precipitates that formed contain porous MOFs.

4. Sorption Studies of Polyaromatic Hydrocarbons by MOFs

Crystal structures of Yaghi's IRMOF-5 and our Cd MOF-2 (Figure 16) show that these frameworks consist of hydrophilic metal centers (highlighted in yellow) generated by coordinated oxygen atoms and hydrophobic walls (highlighted in blue) consisting of the aromatic backbones of the linking ligands. Analysis of space-filling models of those structures revealed that the hydrophilic centers are buried within the hydrophobic walls and that the channel walls appear largely hydrophobic in nature. Therefore, we hypothesized that those MOFs would exhibit high affinity for sorption of hydrophobic guest molecules from a solution.

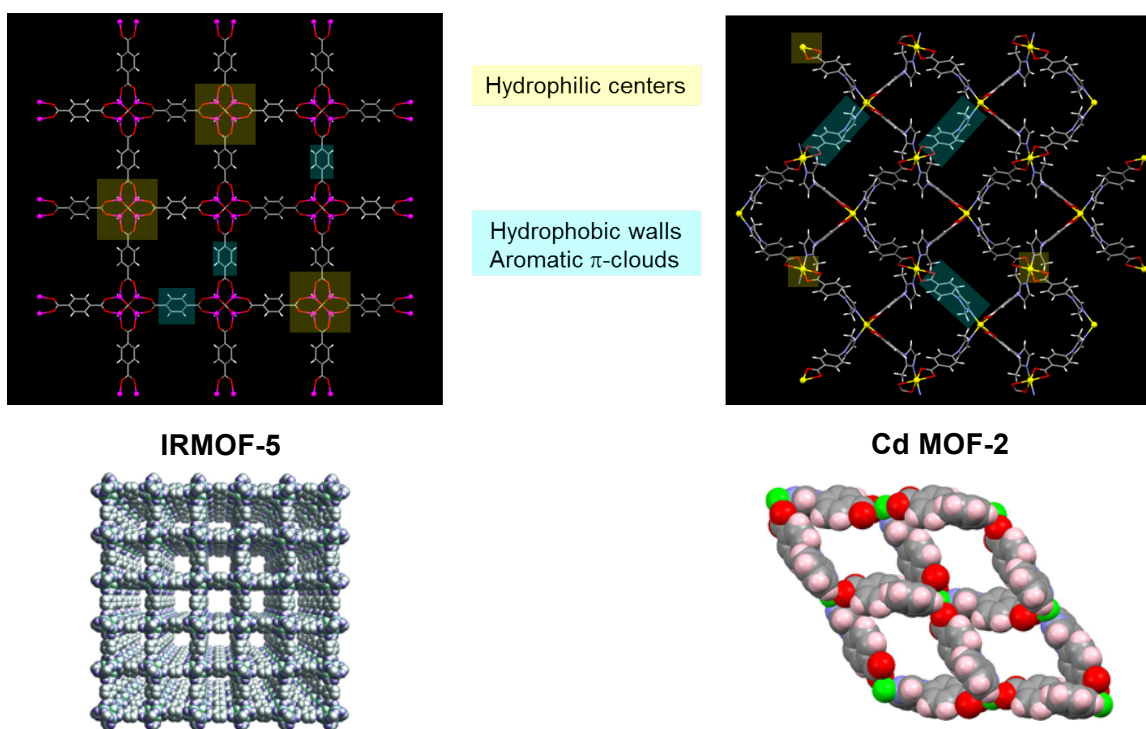


Figure 16. Cap-and-stick (top) and space-filling (bottom) views of the crystal structures and channels of IRMOF-5 and Cd MOF-2.

To validate this hypothesis, a set of hydrophobic guests was chosen for sorption experiments by IRMOF-5 and Cd MOF-2. Polyaromatic hydrocarbons (PAHs) are hydrophobic hydrocarbons that consist of fused aromatic rings.^[18] Three PAHs were chosen for this study—naphthalene, phenanthrene and pyrene—because (1) they are hydrophobic, (2) they have dimensions comparable to that of the MOF channels, and (3) they increase incrementally in length and width, making them a suitable set of guests to investigate surface interactions with the walls of the channels. Another reason for investigating the sorption of PAHs was to test the potential of using MOFs in environmental remediation. PAHs are widespread carcinogenic

pollutants that are present in processed fossil fuels, asphalt and water tables. The structures and relevant physical data for naphthalene, phenanthrene and pyrene are shown in Figure 17.

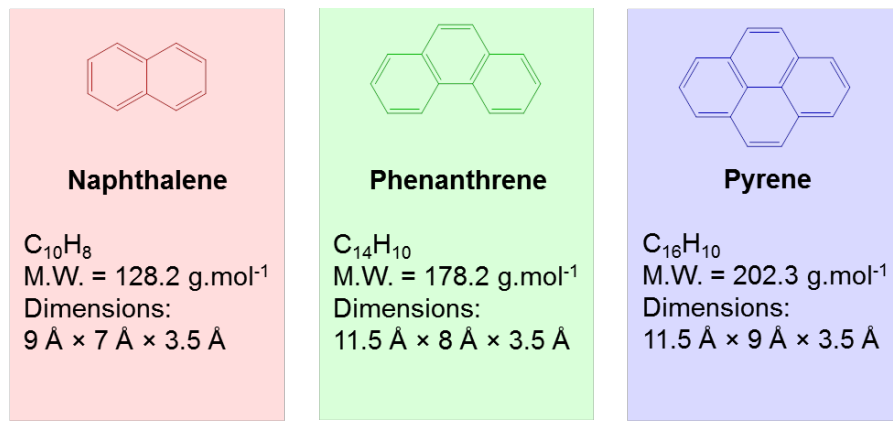


Figure 17. Chemical structures, formulas, molecular weights, and molecular dimensions for naphthalene, phenanthrene, and pyrene.

We chose to investigate IRMOF-5 and Cd MOF-2 as host sorbants based for several reasons. IRMOF-5 features large 13 Å × 13 Å channels that result in a solvent accessible surface area of 3774 m²/g and void volume of 8.3 × 10⁻⁸ m³/g, while Cd MOF-2 features smaller 10 Å × 4 Å channels with a solvent accessible surface area of 617 m²/g and void volume of 3.0 m³/g. Considering that both frameworks exhibit large surface areas consisting primarily of aromatic linkers, it is likely that both MOFs would actively adsorb significant quantities of PAHs via van der Waals interactions onto the exposed aromatic surfaces. Moreover both MOFs feature channels with dimensions large enough to admit all three PAHs via diffusion from solution. It is well established that porous hosts generally show higher affinity for guests with dimensions that closely match the dimensions of the accessible channels due to energetically more favorable interaction between the guest and walls of the channels. Therefore, we anticipated that Cd MOF-2 would show greater affinity for all three PAH guests due to its smaller channels and greater surface area to void volume ratio compared to IRMOF-5. Lastly, we chose to include IRMOF-5 in order to compare the sorption behavior of one of our lower symmetry, 4-(imidazol-1-yl)benzoic acid based MOF systems to that of the well-established cubic, BDC-based IRMOF-5. It is worth mentioning that although IRMOF-5 represents the most well investigated MOF systems to date, reported studies of sorption with that system have focused largely on the ability of IRMOF-5 to take up gases such as hydrogen and low-molecular weight saturated hydrocarbons such as methane. Therefore, we wanted to examine the sorption behavior of IRMOF-5 with regard to larger aromatic hydrocarbon guest.

4.1. Methodology

Solutions of the three PAHs were prepared in ethanol over a range of concentrations. The concentration range for naphthalene and phenanthrene was 2.0 – 20.0 mM, while the concentration range for the pyrene was 0.2 – 6.0 mM. Higher concentrations of pyrene were not used to avoid aggregate formation and problems with UV detection associated with the high molar absorptivity of pyrene. The concentrations of solutions were measured by liquid chromatography using an Agilent 1100 LC-MS equipped with a C-18 column and UV-Vis detector. Calibration curves were generated by plotting the areas of peak against the concentrations of PAH in ethanol across the range of concentration.

IRMOF-5 was synthesized for the sorption experiments at room temperature following a procedure published by L. Huang et al.^[19] MOF powders were activated to maximize sorption of guests by heating samples of MOF solids to 120°C under vacuum for at least two days to ensure removal of any solvent remaining in the channels. Solutions of samples for sorption were prepared in 2.0 mL Agilent LC vials with a rubber septum caps. Activated MOF powder (50 mg) was added to the LC vials along with 1.00 mL of PAH solution at a given concentration. The vial was then immediately placed on the LC sequencing tray along with vials of same PAH solutions at different concentration, all containing 50 mg of the same MOF. The LC instrument then injected 5.0 µL aliquots from each vial into the column at different times to measure the concentrations of PAH remaining in solution. An example of the sampling sequence used is shown in Figure 18. Temperature and distribution of particle size were kept constant throughout the experiments.

	time (arbitrary units)	t ₁					t ₂					t ₃				
		0	2	4	6	8	10	12	14	16	18	20	22	24	26	28
Position on tray	Vial 1	•					•					•				
	Vial 2		•					•					•			
	Vial 3			•					•					•		
	Vial 4				•					•					•	
	Vial 5					•					•					•

Figure 18. Example of the Liquid-Chromatography sequence for five vials of PAH guest solutions with increasing concentrations; the injector position is indicated by the dots at different times.

4.2. Results and Discussion

Sorption Kinetics and Equilibria

The kinetics of sorption processes can be very complex and take into consideration the mass transfer within the boundary layer around the sorbent and in the pores or along the walls of the sorbent. Typical models for sorption usually consider both external and internal mass transfer such as the film-pore diffusion and film-surface diffusion. These models require complex computations of diffusion

coefficients.^[20] Therefore, for simplicity and practical use in engineering applications, the pseudo-second-order rate equation was used to describe the sorption kinetics.^[21]

Pseudo-second-order rate equation:

$$\frac{dq_t}{dt} = k(q_e - q_t)^2$$

Where q_t is the number of moles sorbed, k is a rate constant and q_e is the equilibrium number of moles sorbed. The integral of this equation describes the increase in moles sorbed with time:

$$q_t = \frac{kq_e^2 t}{1 + kq_e t}$$

The linearized equation is used to find the constants from the correlation between t/q_t and t :

$$\frac{t}{q_t} = \frac{1}{kq_e^2} + \frac{t}{q_e}$$

Where the slope of the line is $1/q_e$ and the intercept is $1/kq_e^2$. These values were obtained for each set of data from the plot of t/q_t against t , as shown in Figure 19 for naphthalene.

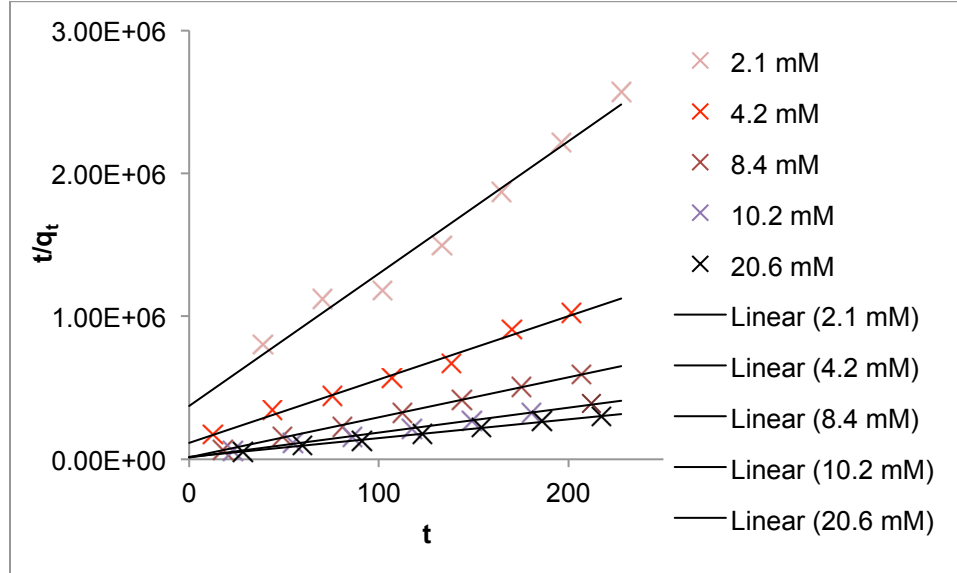


Figure 19. Plot of t/q against t for the sorption data for naphthalene.

The q_t values were calculated from the concentrations of the solutions by the equation:

$$q_t = V_0 C_0 - V_f C_f - V_{inj} \sum_k^n C_k$$

Where V_0 and C_0 are the initial volume and concentration respectively, V_f and C_f are the final volume and concentration respectively, V_{inj} is the volume injected by the LC injector, which was kept constant at 5.0 μL for all measurements, and C_k is the concentration of the solution during the time of injection.

The constants obtained for each set of data for a given starting concentration were then used to plot the increase in moles sorbed with time. The goodness of fit was measured by the R^2 value, which was calculated for each set of data by the equation:

$$R^2 = 1 - \left[\frac{\sum (q_{t,exp} - q_{t,calc})^2}{\sum (q_{t,exp} - q_{t,mean})^2} \right]$$

The experimental results for sorption of the three PAHs in IRMOF-5 are shown in Figures 20-22 and Tables 2-4, along with the pseudo-second-order model curves used to fit the data, and the associated constants and R^2 values.

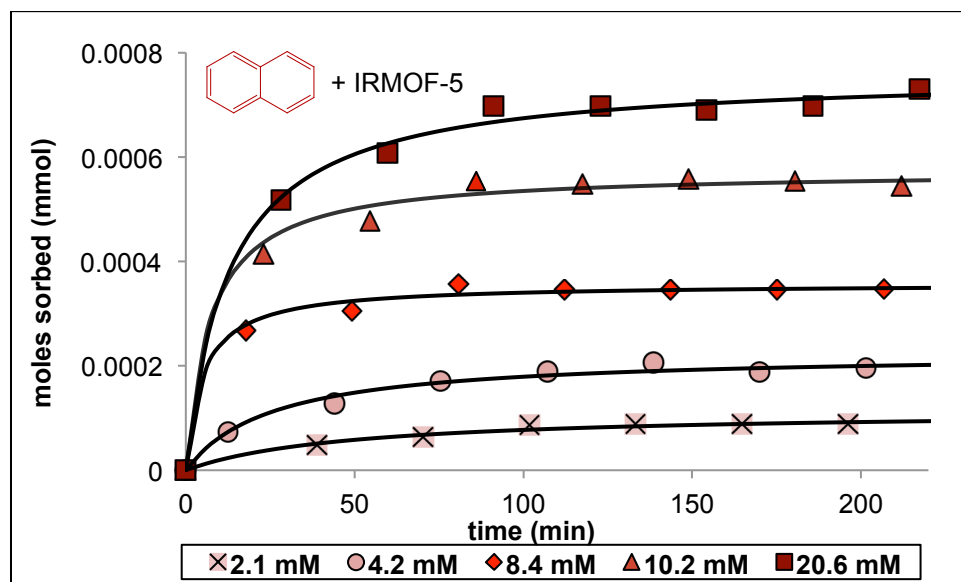


Figure 20. Pseudo-second-order sorption kinetics of naphthalene by IRMOF-5.

Table 2. Pseudo-second-order model constants for the sorption of naphthalene by IRMOF-5 and the R^2 values.

C_0 (mM)	2.1	4.2	8.4	10.2	20.6
q_e (mmol)	1.15×10^{-4}	2.25×10^{-4}	3.57×10^{-4}	5.74×10^{-4}	7.61×10^{-4}
k (mmol $^{-1}$.min $^{-1}$)	179.47	171.22	554.02	240.08	102
R^2	0.94	0.96	0.95	0.95	0.98

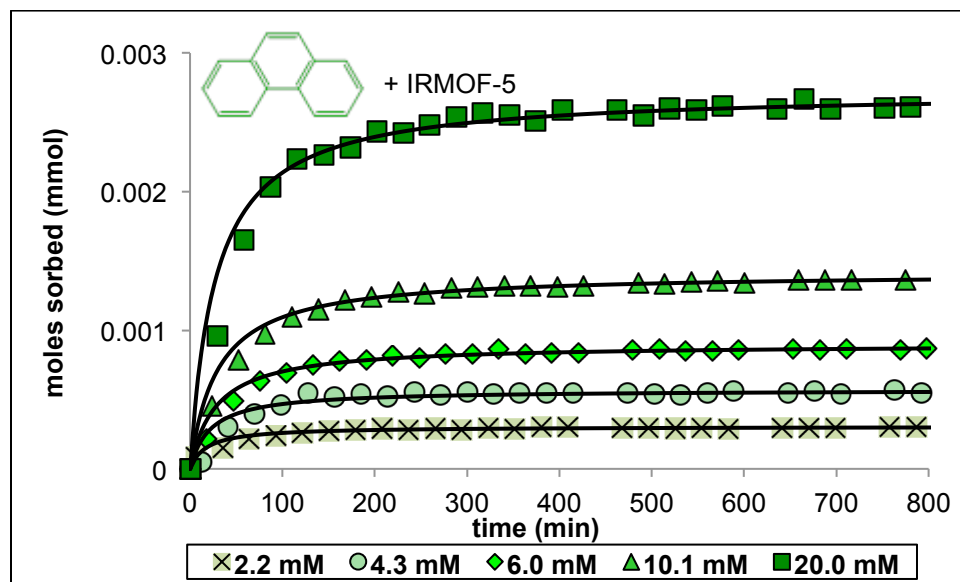


Figure 21. Pseudo-second-order sorption kinetics of phenanthrene by IRMOF-5.

Table 3. Pseudo-second-order model constants for the sorption of phenanthrene by IRMOF-5 and the R^2 values.

C_0 (mM)	2.2	4.3	6.0	10.1	20.0
q_e (mmol)	3.05×10^{-4}	5.70×10^{-4}	8.99×10^{-4}	1.42×10^{-3}	2.72×10^{-3}
k (mmol $^{-1}$.min $^{-1}$)	184.88	80.14	39.61	23.95	13.36
R^2	0.96	0.94	0.98	0.98	0.96

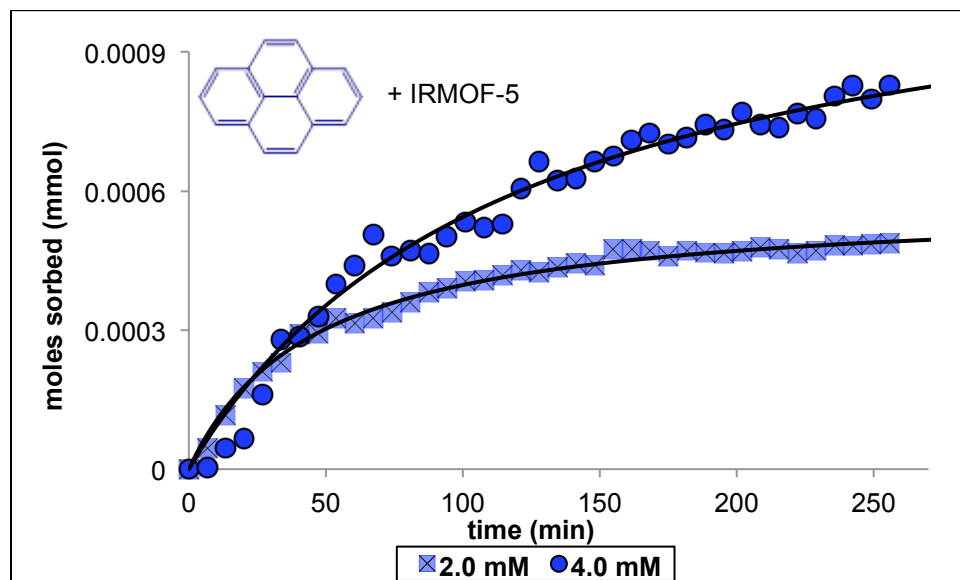


Figure 22. Pseudo-second-order sorption kinetics of pyrene by IRMOF-5.

Table 4. Pseudo-second-order model constants for the sorption of pyrene by IRMOF-5 and the R^2 values.

C_0 (mM)	2.0	4.0
q_e (mmol)	5.78×10^{-4}	2.25×10^{-4}
k (mmol $^{-1}$.min $^{-1}$)	38	171.22
R^2	0.99	0.98

Analysis of the data clearly indicates that sorption of the PAH guests by IRMOF-5 was an equilibrium process because of the asymptotic number of moles sorbed, q_e , that was reached after long time intervals. The plots in Figures 20-22 show that the number moles of PAH guest sorbed was higher for higher initial concentrations. Therefore, the Langmuir equilibrium adsorption isotherm was used to model the equilibrium number of moles sorbed:

$$q_e = \frac{Q_L K_L C_e}{1 + K_L C_e}$$

Where q_e is the equilibrium number of moles sorbed at different initial concentrations and C_e is the concentration of the solution that is in equilibrium with the amount (moles) of PAH guest sorbed. Q_L and K_L are Langmuir isotherm constants. The equilibrium concentration was calculated by the equation:

$$C_e = \frac{C_0 V_0 - q_e}{V_0}$$

The Langmuir isotherm constants were calculated from the linearized Langmuir equation:

$$\frac{C_e}{q_e} = \frac{1}{Q_L K_L} + \frac{C_e}{Q_L}$$

Where the slope of the line is $1/Q_L$ and the intercept is $1/Q_L K_L$. These values were obtained for each set of data by plotting C_e/q_e against C_e . The Langmuir isotherms obtained for the three PAHs in IRMOF-5 and associated Langmuir constants are shown in Figure 23 and Table 5.

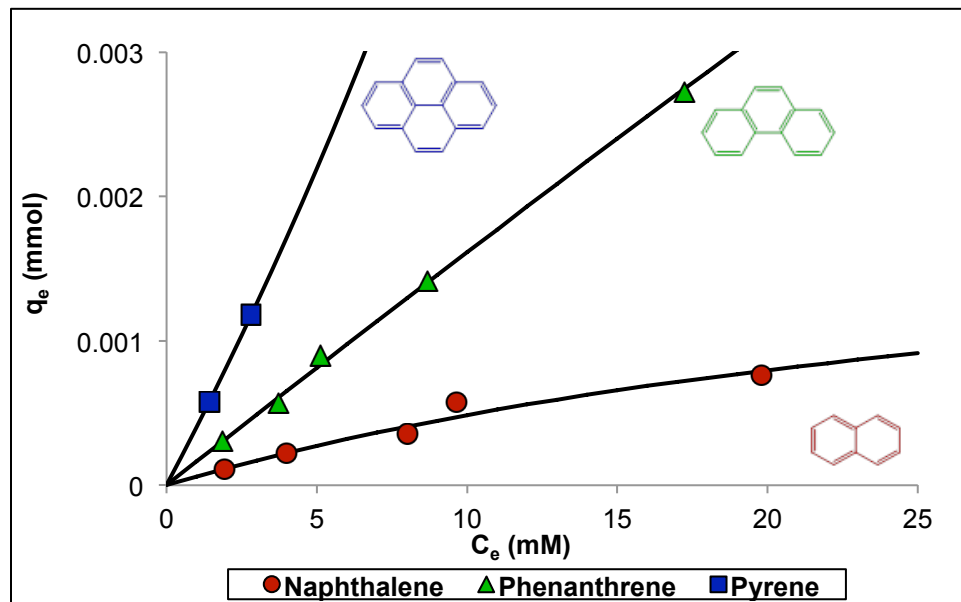


Figure 23. Langmuir isotherms for the sorption of three PAHs by IRMOF-5

Table 5. Langmuir model constants for the sorption of three PAHs by IRMOF-5 and the R^2 values

	Naphthalene	Pheneanthrene	Pyrene
K_L (mmol.mM ⁻¹)	2.83×10^{-2}	1.92×10^{-3}	-1.99×10^{-2}
Q_L (mmol)	2.21×10^{-3}	8.58×10^{-2}	-1.99×10^{-2}
R^2	0.95	0.998	0.99

The data shown in Figure 23 provides convincing evidence supporting our hypothesis that MOF channels are hydrophobic and will sorb hydrophobic PAH guests. The higher sorption of guests with larger cross-sectional area further indicates that the guests are interacting with the walls, with larger guests showing higher affinity that leads to enhanced sorption. Although only two data points (in addition to the point at the origin) were determined for pyrene due to aggregation of pyrene in solution and problems with accurate UV detection at higher concentrations, the data is consistent with higher sorption of larger guests observed for phenanthrene compared to naphthalene.

A similar set of sorption experiments was performed to examine sorption of the three PAHs by Cd MOF-2. The same analysis was performed on the sorption data and similar results were obtained. The experimental results for sorption in Cd MOF-2 are shown in Figures 24-26 and Tables 6-8, along with the pseudo-second-order model curves used to fit the data, and the associated constants and R^2 values.

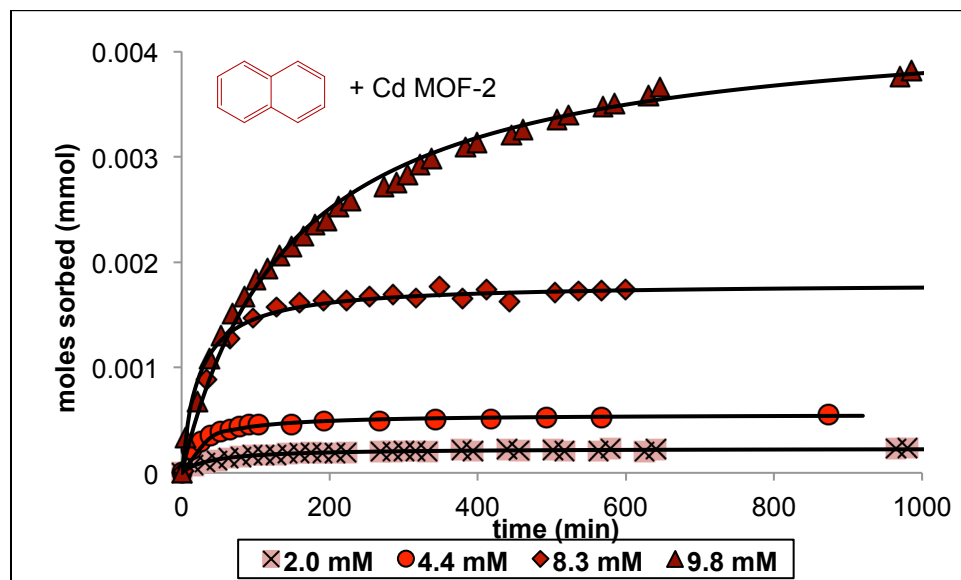


Figure 24. Pseudo-second-order sorption kinetics of naphthalene by Cd MOF-2

Table 6. Pseudo-second-order model constants for the sorption of naphthalene by Cd MOF-2 and the R^2 values

C_0 (mM)	2.0	4.4	8.3	9.8
q_e (mmol)	2.32×10^{-4}	5.57×10^{-4}	1.80×10^{-3}	4.35×10^{-3}
k ($\text{mmol}^{-1} \cdot \text{min}^{-1}$)	107.69	69.82	24.3	1.56
R^2	0.96	0.99	0.98	0.99

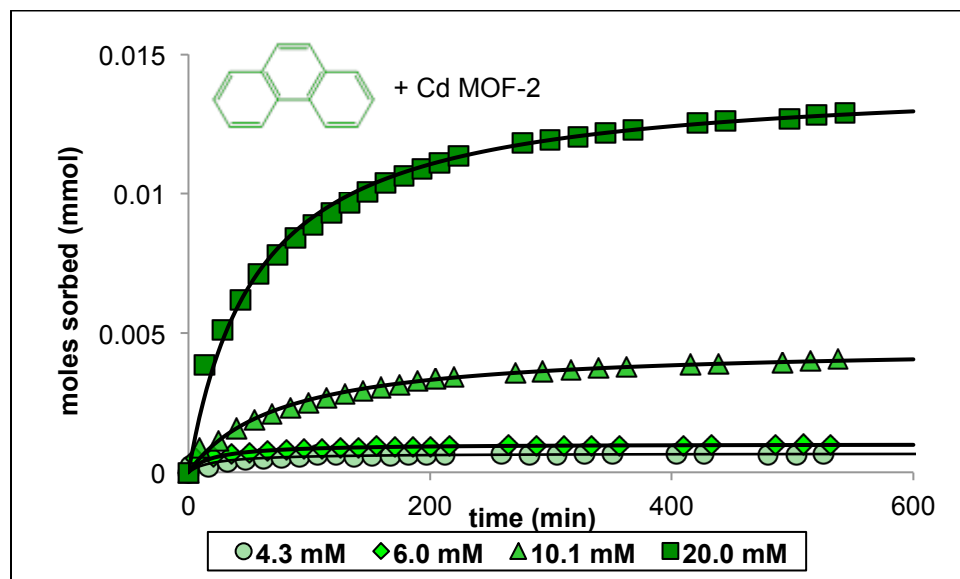


Figure 25. Pseudo-second-order sorption kinetics of phenanthrene by Cd MOF-2

Table 7. Pseudo-second-order model constants for the sorption of phenanthrene by Cd MOF-2 and the R² values

C ₀ (mM)	4.3	6.0	10.1	20.0
q _e (mmol)	6.81 × 10 ⁻⁴	1.02 × 10 ⁻³	4.56 × 10 ⁻³	1.42 × 10 ⁻²
k (mmol ⁻¹ .min ⁻¹)	72.52	49.47	2.91	1.25
R ²	0.96	0.94	0.98	0.98

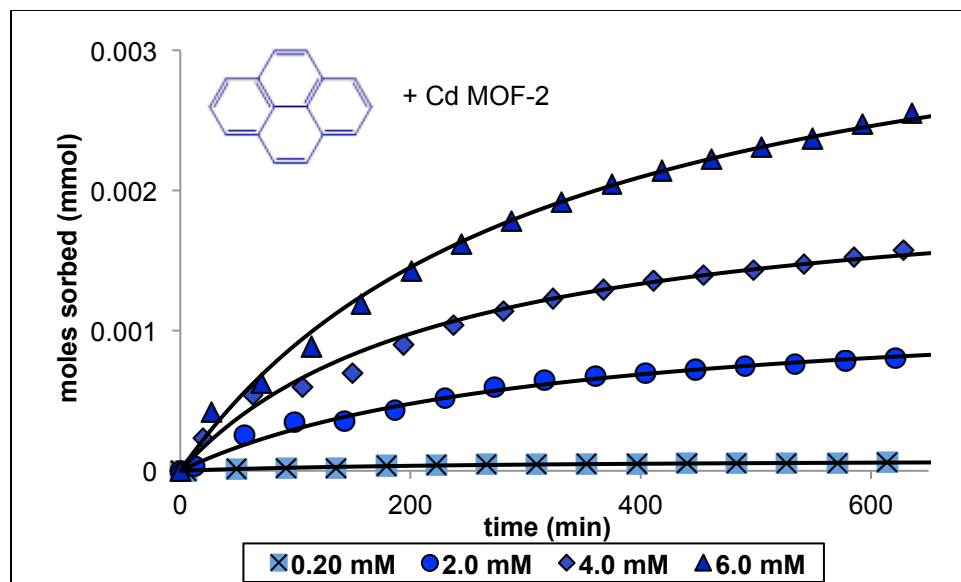


Figure 26. Pseudo-second-order sorption kinetics of pyrene by Cd MOF-2

Table 8. Pseudo-second-order model constants for the sorption of pyrene by Cd MOF-2 and the R² values

C ₀ (mM)	0.2	2.0	4.0	6.0
q _e (mmol)	8.51 × 10 ⁻⁵	1.22 × 10 ⁻³	2.10 × 10 ⁻³	3.77 × 10 ⁻³
k (mmol ⁻¹ .min ⁻¹)	42.43	2.63	2.07	0.83
R ²	0.97	0.98	0.97	0.99

The Langmuir isotherms obtained from the equilibrium number of moles sorbed and the calculated equilibrium concentrations for the three PAHs in Cd MOF-2 and associated Langmuir constants are shown in Figure 27 and Table 9.

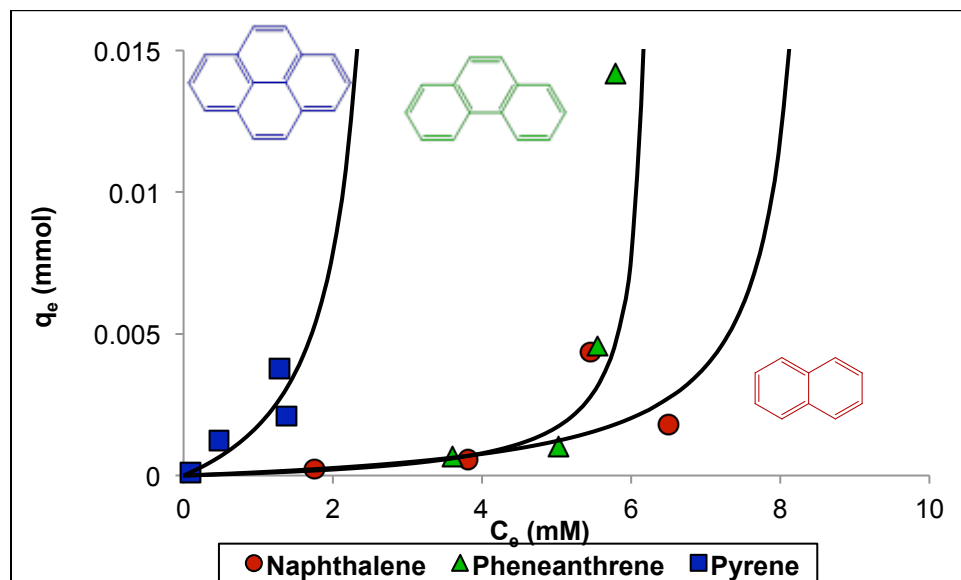


Figure 27. Langmuir isotherms for the sorption of three PAHs by Cd MOF-2

Table 9. Langmuir model constants for the sorption of three PAHs by Cd MOF-2 and the R^2 values

	Naphthalene	Phenanthrene	Pyrene
K_L ($\text{mmol}\cdot\text{mM}^{-1}$)	-1.16×10^{-1}	-1.57×10^{-1}	-3.55×10^{-1}
Q_L (mmol)	-8.73×10^{-4}	-4.63×10^{-4}	-3.20×10^{-3}
R^2	0.72	0.9	0.88

Although the isotherms for sorption of naphthalene, phenanthrene, and pyrene by Cd MOF-2 behave in a different manner mathematically compared to those obtained for IRMOF-5—that is, the Langmuir constants are negative—the general trend is similar to the results obtained for IRMOF-5. As predicted, sorption of the PAH guests at the same initial concentration is consistently higher in Cd MOF-2 compared to IRMOF-5. The higher relative affinity of PAH guests for Cd MOF-2 is consistent with our hypothesis that the smaller $10 \text{ \AA} \times 4 \text{ \AA}$ channels in Cd MOF-2 (vs. $13 \text{ \AA} \times 13 \text{ \AA}$ channels in IRMOF-5) provide a tighter fit that enhances sorption of the PAH guest via hydrophobic van der Waals interactions with the aromatic ligands present on the walls of the channels.

Competitive Sorption Experiments

Competitive sorption experiments between naphthalene and phenanthrene by IRMOF-5 were carried out to determine whether the higher affinity observed for guests with larger surface area would lead to selective sorption of phenanthrene over naphthalene when both PAH guests were present in equimolar amounts in solution. Three solutions containing phenanthrene and naphthalene in a 1:1 molar ratio were prepared at concentrations of 2.0, 3.0 and 5.0 mM for both solutes. Each solution (1.00 mL) was added to

LC vial containing 50 mg of activated IRMOF-5. The vials were left undisturbed for 48 hrs, after which the concentrations of solutions were measured by LC. The linear region of the equilibrium isotherms for both naphthalene and phenanthrene obtained previously predicted that IRMOF-5 would show a three-fold (i.e., 2.9:1) selectivity for phenanthrene over naphthalene, as shown in Figure 28.

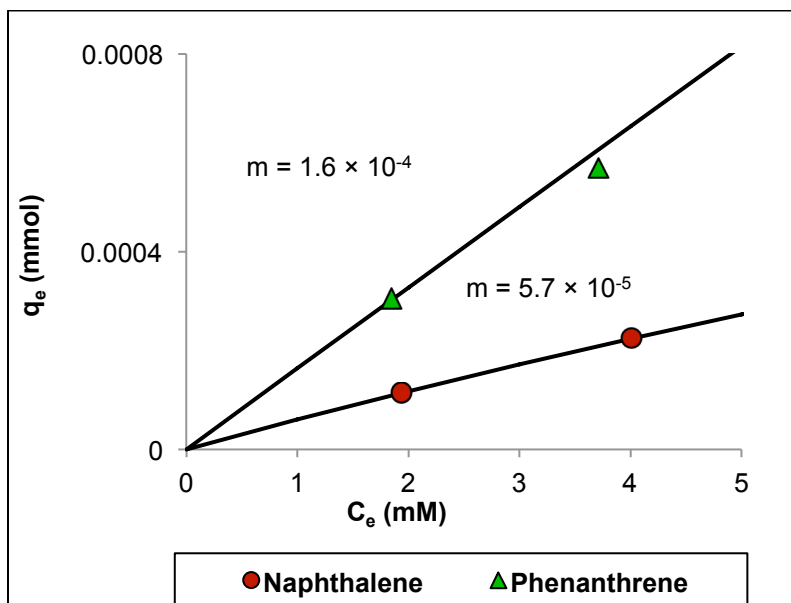


Figure 28. The linear region of the Langmuir isotherms for the sorption naphthalene and phenanthrene by IRMOF-5

The results of the competition experiments at the three concentrations are summarized in Figure 29. In contrast to the predicted selectivity from the equilibrium sorption data, these findings clearly show that IRMOF-5 preferentially sorbs phenanthrene over naphthalene by an average factor of 8.2 ± 0.3 at the concentrations tested. This data indicates that the greater surface area of phenanthrene plays a significant role in promoting stronger binding to the walls of the MOF compared to naphthalene, which has a smaller surface area. Conclusions that can be drawn from these experiments are that sorption of PAH guests by MOFs is not accurately predicted by simply comparing the relative number of moles of PAHs sorbed at equilibrium from single-component solutions at the same concentration. Rather, the affinity of MOFs for different PAHs is affected greatly by the relative surface areas of the molecules such that guests with greater surface area will show enhanced binding. Therefore, assuming the dimensions of the MOF channels are large enough to admit both guests, the degree to which a given MOF exhibits selectivity in sorbing one guest over another at equilibrium will be determined largely by (1) the relative surface areas of the guests, (2) the relative accessible surface area to void volume ratio of the MOF host, and (3) the nature and strength of the intermolecular interactions that form between the guest and the molecular components in the walls of the framework. In cases where the guests are hydrophobic PAH guests, surface area of the guest should predominate in determining selectivity.

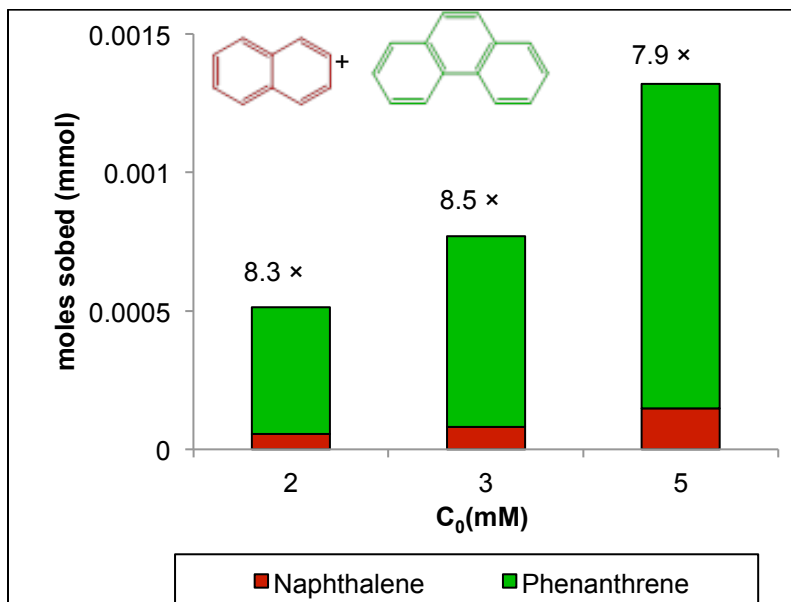


Figure 29. Comparison of the number of moles of naphthalene (red) and phenanthrene (green) sorbed by IRMOF-5

This result showed that MOFs are not only good sorbents that could be utilized in environmental remediation, but also excellent materials for extraction and purification. The results obtained show that with three rounds of sorption and desorption 99.9 mol % purities can be achieved.

5. Conclusions

- Metal-organic frameworks were synthesized using 4-(imidazol-1-yl) benzoate ligands.
- Changing the substituents on the parent ligand gave MOFs with different architectures.
- Changing the substituents on the substituted ligand maintained the MOF architecture.
- PAHs were actively sorbed by IRMOF-5 and Cd MOF-2.
- All MOFs showed higher affinity for larger PAHs.
- MOFs with smaller pores/ higher surface areas showed greater sorption compared to MOFs with larger pores/ lower surface areas.
- IRMOF-5 selectively sorbed phenanthrene (8×) over naphthalene (1×).

6. References

1. Ishizaki, K.; Komarneni, S.; Nanko, M. In *Porous materials: process technology and applications*; Chapman & Hall: 1998; .
2. Hubbard, A. T. In *Encyclopedia of surface and colloid science: A-Dif*; CRC: 2002.
3. Auerbach, S. M.; Carrado, K. A.; Dutta, P. K. In *Handbook of zeolite science and technology*; CRC: 2003.
4. Lastoskie, C.; Gubbins, K. E.; Quirke, N. Pore size distribution analysis of microporous carbons: a density functional theory approach. *J. Phys. Chem.* **1993**, *97*, 4786-4796.
5. Czaja, A. U.; Trukhan, N.; Müller, U. Industrial applications of metal–organic frameworks. *Chem. Soc. Rev.* **2009**, *38*, 1284-1293.
6. a) Gomez-Lor, B.; Gutierrez-Puebla, E.; Iglesias, M.; Monge, M.; Ruiz-Valero, C.; Snejko, N. Novel 2D and 3D indium metal-organic frameworks: Topology and catalytic properties. *Chemistry of materials* **2005**, *17*, 2568-2573.
b) Ma, S.; Yuan, D.; Wang, X. S.; Zhou, H. C. Microporous Lanthanide Metal-Organic Frameworks Containing Coordinatively Linked Interpenetration: Syntheses, Gas Adsorption Studies, Thermal Stability Analysis, and Photoluminescence Investigation. *Inorg. Chem.* **2009**, *48*, 2072-2077.
7. Li, H.; Eddaoudi, M.; O'Keeffe, M.; Yaghi, O. M. Design and synthesis of an exceptionally stable and highly porous metal-organic framework. *Nature* **1999**, *402*, 276-279.
8. Eddaoudi, M.; Kim, J.; Rosi, N.; Vodak, D.; Wachter, J.; O'Keeffe, M.; Yaghi, O. M. Systematic design of pore size and functionality in isorecticular MOFs and their application in methane storage. *Science* **2002**, *295*, 469.
9. Murray, L. J.; Dinca, M.; Long, J. R. Hydrogen storage in metal-organic frameworks. *Chem. Soc. Rev.* **2009**, *38*, 1294-1314.
10. Lee, J. Y.; Farha, O. K.; Roberts, J.; Scheidt, K. A.; Nguyen, S. B. T.; Hupp, J. T. Metal–organic framework materials as catalysts. *Chem. Soc. Rev.* **2009**, *38*, 1450-1459.
11. Uemura, T.; Yanai, N.; Kitagawa, S. Polymerization reactions in porous coordination polymers. *Chem. Soc. Rev.* **2009**, *38*, 1228-1236.
12. Ma, L.; Abney, C.; Lin, W. Enantioselective catalysis with homochiral metal–organic frameworks. *Chem. Soc. Rev.* **2009**, *38*, 1248-1256.
13. Yigit, M. V.; Biyikli, K.; Moulton, B.; MacDonald, J. C. Bis (imidazolium 2, 4, 6-tricarboxypyridine) metal (II) complexes: Molecular building blocks that generate isomorphous hydrogen-bonded frameworks. *Crystal growth & design* **2006**, *6*, 63-69.
14. Nelson, A. P.; Parrish, D. A.; Cambrea, L. R.; Baldwin, L. C.; Trivedi, N. J.; Mulfort, K. L.; Farha, O. K.; Hupp, J. T. Crystal to Crystal Guest Exchange in a Mixed Ligand Metal– Organic Framework. *Crystal Growth & Design* **2009**, *9*, 4588-4591.
15. Morgan Jr, T. K.; Lis, R.; Lumma Jr, W. C.; Nickisch, K.; Wohl, R. A.; Phillips, G. B.; Gomez, R. P.; Lampe, J. W.; Di Meo, S. V. Synthesis and cardiac electrophysiological activity of N-substituted-4-(1H-imidazol-1-yl) benzamides-new selective class III agents. *J. Med. Chem.* **1990**, *33*, 1091-1097.

16. Xu, Y.; Xi, J.; Wei, W.; Chi, Y.; Hu, C. A 3D homochiral framework with rare 49·66 structural topology constructed by unique triple-stranded helices. *Inorganic Chemistry Communications* **2010**, *13*, 852-854.
17. D'Auria, M.; Racioppi, R. Photochemical dimerization of esters of urocanic acid. *J. Photochem. Photobiol. A* **1998**, *112*, 145-148.
18. Fetzer, J. The chemistry and analysis of the large polycyclic aromatic hydrocarbons. *Polycyclic Aromatic Compounds* **2000**, *27*, 143.
19. Huang, L.; Wang, H.; Chen, J.; Wang, Z.; Sun, J.; Zhao, D.; Yan, Y. Synthesis, morphology control, and properties of porous metal-organic coordination polymers. *Microporous and mesoporous materials* **2003**, *58*, 105-114.
20. Babich, I. V.; van Langeveld, A. D.; Zhu, W.; Bakker, W. J. W.; Moulijn, J. A. A rotating adsorber for multistage cyclic processes: Principle and experimental demonstration in the separation of paraffins. *Ind Eng Chem Res* **2001**, *40*, 357-363.
21. Chang, C. F.; Chang, C. Y.; Chen, K. H.; Tsai, W. T.; Shie, J. L.; Chen, Y. H. Adsorption of naphthalene on zeolite from aqueous solution. *J. Colloid Interface Sci.* **2004**, *277*, 29-34.